

Supplemental Information

for

Ru(IV)-Ru(IV) Complexes Having the Doubly Oxido-Bridged Core with a Bridging  
Carbonato or Hydrogencarbonato Ligand

*Tomoyo Misawa-Suzuki\* and Hirotaka Nagao\**

Department of Materials and Life Sciences, Faculty of Science and Technology, Sophia University,  
7-1 Kioi-cho, Chiyoda-ku, Tokyo 102-8554 Japan.

*E-mail; t\_misawa@sophia.ac.jp*

## **Table of Contents**

### **I. Characterization of complexes**

<b>I-1. NMR spectrometry .....</b>	S3
<b>I-2. UV-vis-NIR spectrometry .....</b>	S3
<b>I-3. IR spectroscopy .....</b>	S7
<b>I-4. Electrochemistry .....</b>	S8
<b>II. X-ray crystallography .....</b>	S12
<b>III. UV-vis-NIR spectra in various organic solvents at 298 K.....</b>	S15
<b>IV. Spectroscopic studies on oxidation of C-H bond of ring organic compounds.....</b>	S24
<b>V. DFT Calculations.....</b>	S31
<b>VI. References .....</b>	S34

## I. Characterization of complexes

### I-1. NMR spectrometry

$^1\text{H}$  NMR measurements were performed (-15 – 35 ppm) at 25 °C with a JEOL JML-AL300 spectrometer using sample tubes of  $\phi = 5$  mm. Although all the signals were observed in the diamagnetic region for  $^1\text{H}$  NMR, due to the broadening, further assignment could not be performed.

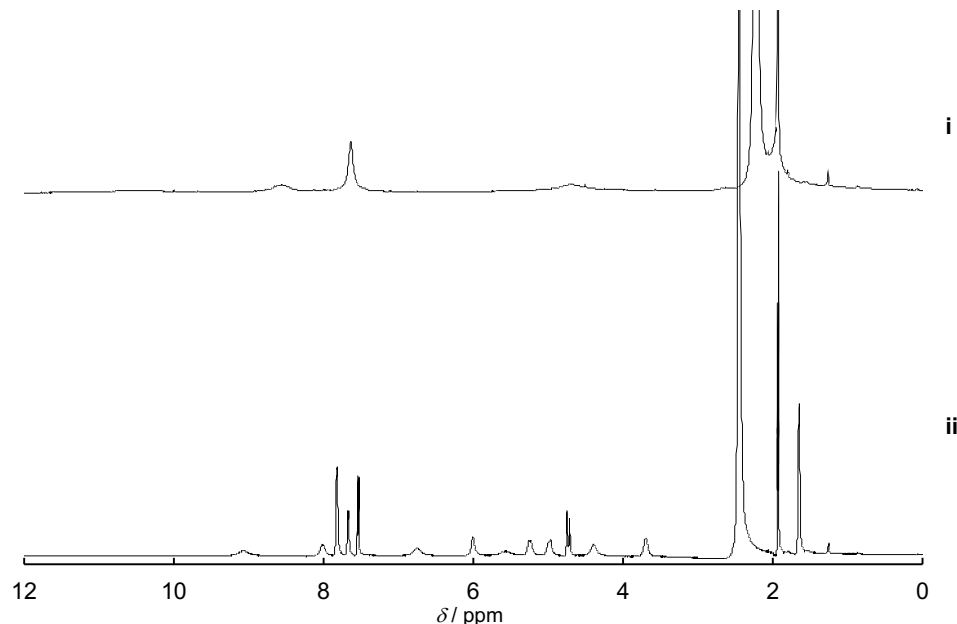


**Figure S1.**  $^1\text{H}$  NMR spectra of  $[\text{IV},\text{IV}]^{2+}$  (i) and  $[\text{IV},\text{IV}_1\text{H}]^{3+}$  (ii) in  $\text{CD}_3\text{CN}$ .

### I-2. UV-vis-NIR spectrometry

UV-vis and Near-IR (NIR) spectra were measured on a Shimadzu UV-3600 Plus or UV-1900i spectrophotometer at 25 °C using a quartz cell with an optical path length of 1 cm.

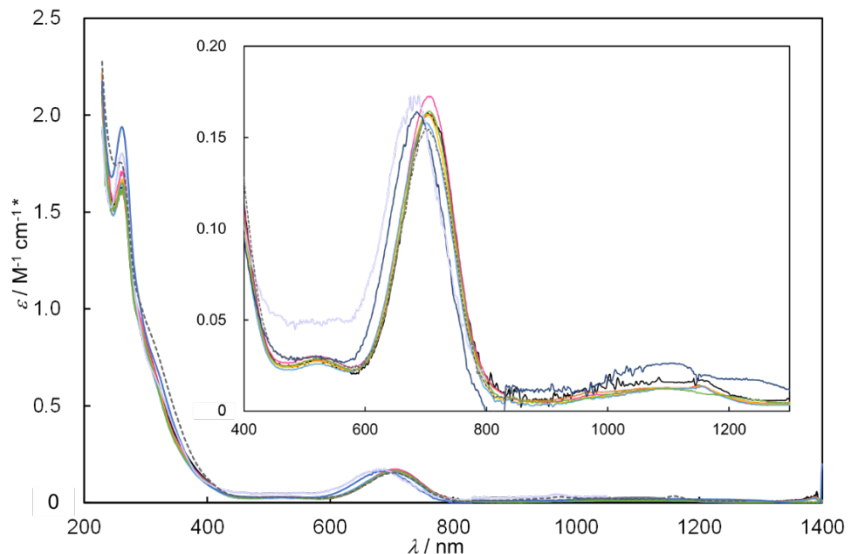


**Figure S2.** UV-vis-NIR spectra in water at pH 5.23 (black), 2.98 (yellow-green line), 2.56 (orange line), 1.96 (pink line), 1.48 (yellow line), 1.25 (blue line), 0.73 (navy line), and 0.55 (purple line). The gray dotted line shows the one after a change from pH 0.55 to 3.65. \*pH 0.73, 0.55, and 3.65 are shown in arbitrary unit.

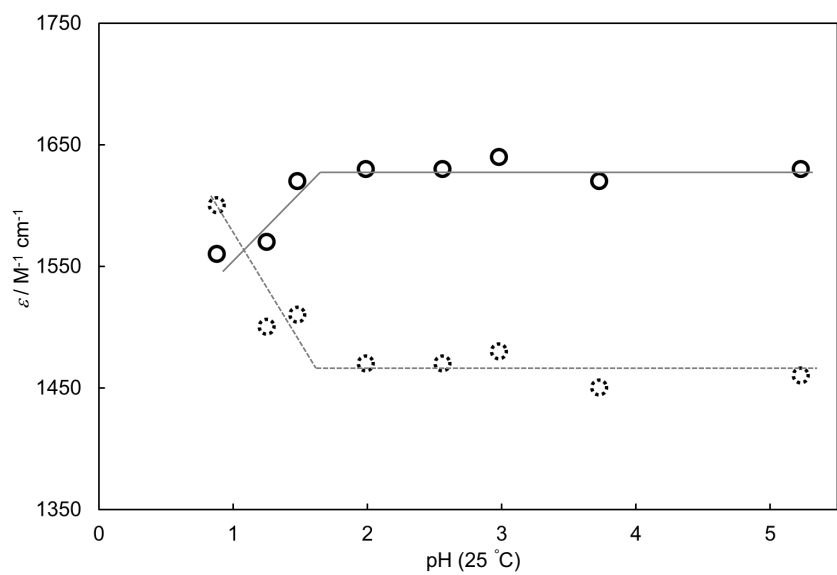


**Figure S3.** Plots of  $\varepsilon / M^{-1} \text{mol}^{-1}$  at 703 nm (solid circle;  $[\text{IV,IV}]^{2+}$ ) and 685 nm (dotted circle;  $[\text{IV,IV\_1H}]^{3+}$ ) in  $\text{HClO}_4(\text{aq.})$ .

**Table S1.** Spectroscopic data in acetonitrile and aqueous solutions of different pH.

in CH <sub>3</sub> CN				
[IV,IV] <sup>2+</sup>		around 242 (21,200)	around 440 (1,170), 538 (590)	762 (1440)
[IV,IV_1H] <sup>3+</sup>		260	-	669 (1970)
[III,IV] <sup>+</sup>		249 (10400)	362 (6900)	1,067 (660), around 1,200
[III,IV_1H] <sup>2+</sup>		246 (17700)	337 (11800)	972 (1,490)
[III,IV_2H] <sup>3+</sup>		246 (19100)	336 (11600)	964 (1,330), around 1,090 (150)
in H <sub>2</sub> O				
[IV,IV] <sup>2+</sup>	pH 5.23	260 (16300)	703 (1630)	around 1,080 (180)
	pH 3.73	261 (16100)	702 (1630)	around 1,095 (90)
	pH 2.98	263 (16500)	706 (1640)	around 1,100 (120)
	pH 2.56	261 (16100)	708 (1630)	around 1,090 (130)
	pH 1.99	261 (16300)	702 (1630)	around 1,095 (110)
	pH 1.48	262 (16700)	701 (1630)	around 1,100 (130)
[IV,IV_1H] <sup>3+</sup>	pH 1.25	261 (16500)	700 (1580)	around 1,100 (120)
	pH 0.88	261 (17900)	690 (1630)	around 1,100 (-)
	pH 0.55	261	681	-
	pH 0.55 to 3.65	259	705	-
[III,IV] <sup>+</sup>	pH 13.2	247 (11700)	335 (7750)	1,035 (820), around 1280 nm
	pH 10.0	247 (11600)	335 (7760)	1,035 (770), around 1280 nm
	pH 6.3	247 (12300)	337 (8190)	1,035 (800), around 1280 nm
[III,IV_1H] <sup>2+</sup>	pH 3.9	245 (13000)	329 (8150)	974 (650), around 1200 nm
[III,IV_2H] <sup>3+</sup>	pH 1.0	244 (10300) 267 (9780)	around 298, 323 nm	1,170 (570)

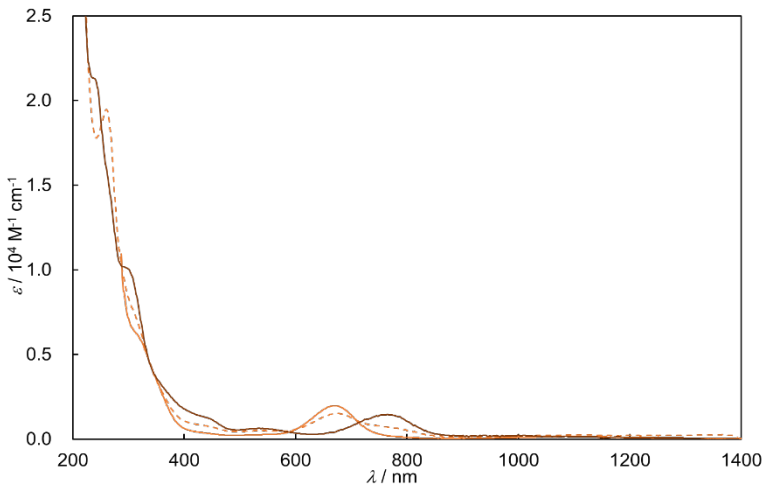


**Figure S4.** UV-vis-NIR spectra of  $[\text{IV},\text{IV}]^{2+}$  (brown line) and  $[\text{IV},\text{IV}_1\text{H}]^{3+}$  (solid orange line) in acetonitrile. The broken orange line is a transient spectrum of a ten-times diluted solution of  $[\text{IV},\text{IV}_1\text{H}]^{3+}$  to change into  $[\text{IV},\text{IV}]^{2+}$ .

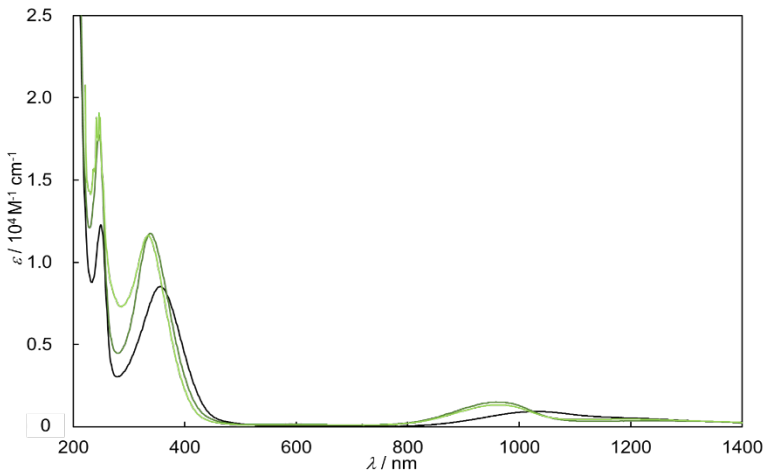


**Figure S5.** UV-vis-NIR spectra of  $\{\text{K}^+ + [\text{III},\text{IV}]^+\}^{\text{S4}}$  (black line),  $[\text{III},\text{IV}_1\text{H}]^{2+}$  (dark green line) and  $\{\text{Na}^+ + [\text{III},\text{IV}_2\text{H}]^{3+}\}$  (yellow green line) in acetonitrile.

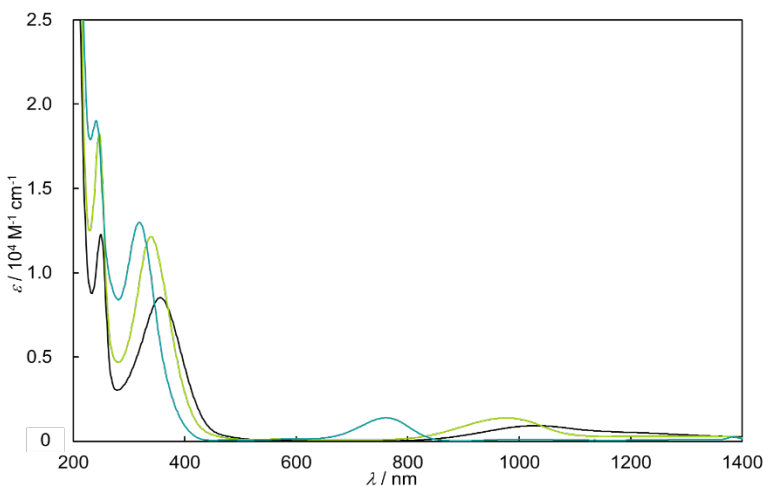


**Figure S6.** UV-vis-NIR spectra of  $\{\text{K}^+ + [\text{III},\text{IV}]^+\}^{\text{S4}}$  (black line),  $[\{\text{Ru}^{\text{III,IV}}(\text{L})\}_2(\mu-\text{O})_2(\mu-\text{O}_2\text{CCH}_3)]^{2+}$  (yellow green line) and  $[\{\text{Ru}^{\text{III,IV}}(\text{L})\}_2(\mu-\text{O})_2(\mu-\text{O}_2\text{NO})]^{2+}$  (blue green line) in acetonitrile.

### I-3. IR spectroscopy

IR spectra were recorded on a Shimadzu IR Affinity-1 spectrophotometer using samples prepared as KBr disks. The integration was done for sixteen times with  $2.0\text{ cm}^{-1}$  resolution.

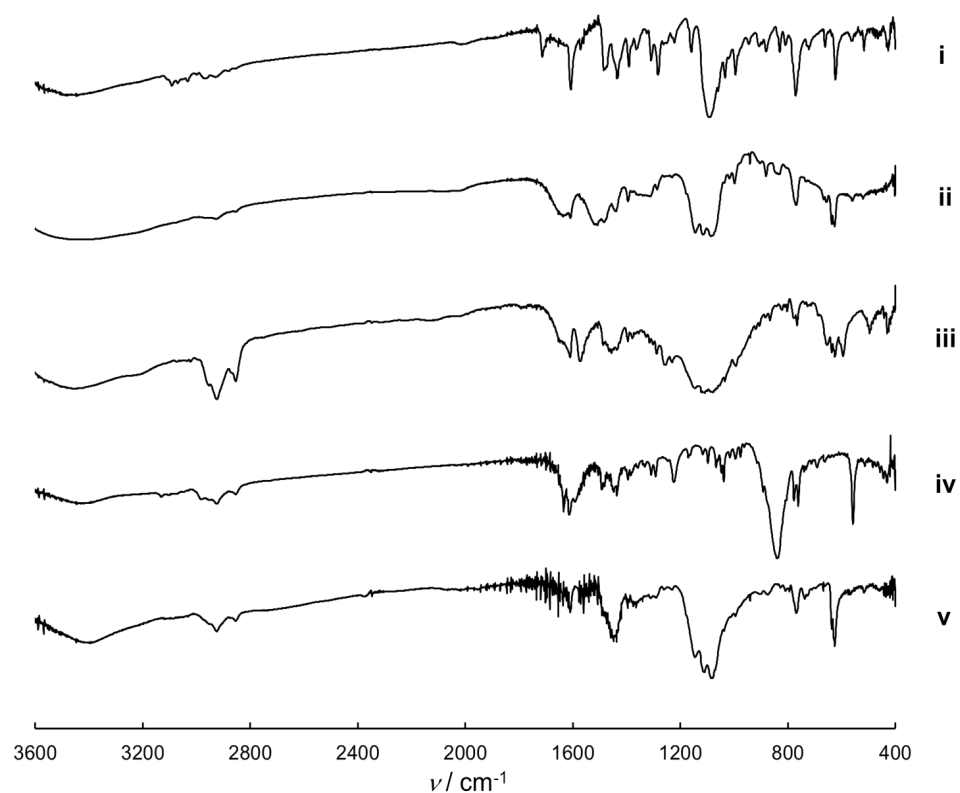


**Figure S7.** IR spectra of (i)  $\{\text{Ru}^{\text{III,IV}}\text{Cl}_2(\text{ebpma})\}_2(\mu\text{-O})\text{ClO}_4 \cdot 0.75(\text{CH}_3)_2\text{CO}$  for a reference, (ii)  $\text{Na}[\text{III,IV}]_2(\text{ClO}_4)_3 \cdot 17\text{H}_2\text{O}$ <sup>S4)</sup> (iii)  $[\text{IV,IV}](\text{ClO}_4)_2 \cdot 2\text{H}_2\text{O}$ , (iv)  $[\text{IV,IV}](\text{PF}_6)_2 \cdot 1.5\text{H}_2\text{O}$  and (v)  $[\text{IV,IV\_1H}](\text{ClO}_4)_3 \cdot \text{HClO}_4 \cdot 7\text{H}_2\text{O}$  (KBr method).

#### I-4. Electrochemistry

All electrochemical measurements were performed by an ALS 630E Electrochemical Analyzer, in which the scan rate is 100 mV s<sup>-1</sup>. In CH<sub>3</sub>CN solutions containing 0.1 M tetra-*n*-butylammonium perchlorate (TBAP, Nakarai Tesque. Ltd.) as a supporting electrolyte, a glassy carbon electrode ( $\phi = 1.6$  mm) and an Ag | 0.01 M AgNO<sub>3</sub> (CH<sub>3</sub>CN) reference electrode were used. At the end of each measurement, ferrocene ([Fe<sup>III</sup>Cp<sub>2</sub>]<sup>+</sup> / [Fe<sup>II</sup>Cp<sub>2</sub>] 0.074 V in CH<sub>3</sub>CN vs. Ag | 0.01 M AgNO<sub>3</sub> (CH<sub>3</sub>CN)) was added as an internal standard to correct redox potentials. In (CH<sub>3</sub>)<sub>2</sub>CO – HClO<sub>4</sub> – NaOH (aq.) aqueous solutions ( $v/v = 1/3$ ), a glassy carbon working electrode ( $\phi = 1.0$  mm) and Ag | AgCl 3.0 mol dm<sup>-3</sup> NaCl reference electrode were used. Cyclic voltammograms were measured in CH<sub>3</sub>CN for [IV,IV]<sup>2+</sup>, [IV,IV\_1H]<sup>3+</sup>, {Na<sup>+</sup> + [III,IV]<sup>+</sup>}<sup>S4)</sup>, [III,IV\_1H]<sup>2+</sup>, and {Na<sup>+</sup> + [III,IV\_2H]<sup>3+</sup>} by using a glassy carbon working electrode ( $\phi = 1.6$  mm). Wave analyses were performed with different scan rates (limiting current  $i_d$  vs. square root of rpm,  $\omega^{1/2}$ ) to ensure that these voltammograms were diffusion limited Faradaic currents, which is worth discussing the reversibility of each wave.

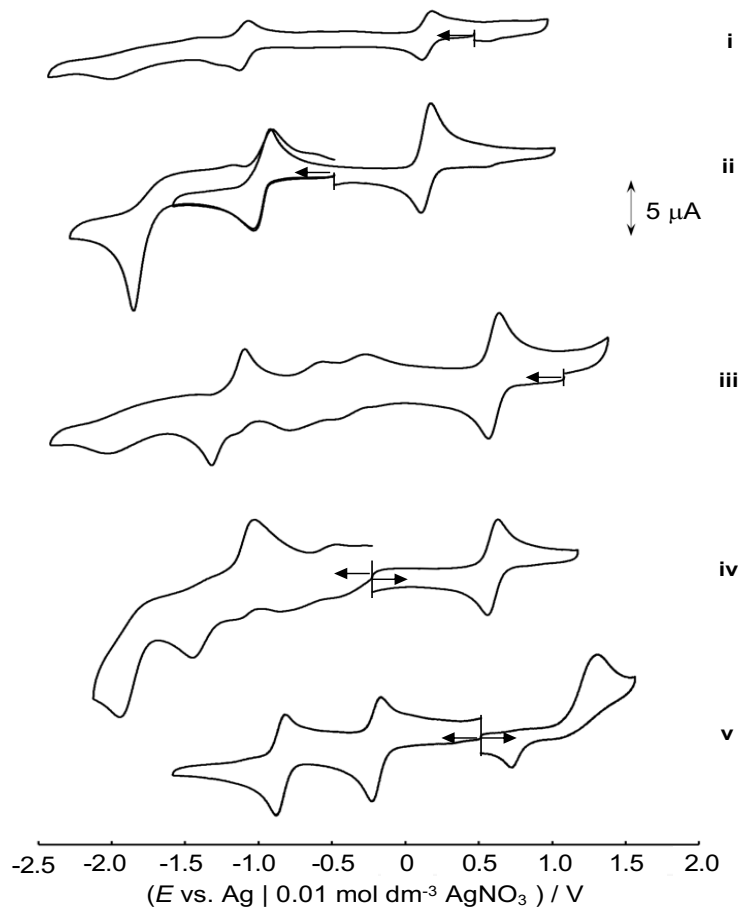


**Figure S8.** Cyclic voltammograms of (i) [IV,IV]<sup>2+</sup> (0.66 mM), (ii) {Na<sup>+</sup> + [III,IV]<sup>+</sup>}<sup>S4)</sup> (1.0 mM), (iii) [IV,IV\_1H]<sup>3+</sup> (1.0 mM), (iv) [III,IV\_1H]<sup>2+</sup> (0.97 mM) and (v) {Na<sup>+</sup> + [III,IV\_2H]<sup>3+</sup>} (1.0 mM) in acetonitrile.

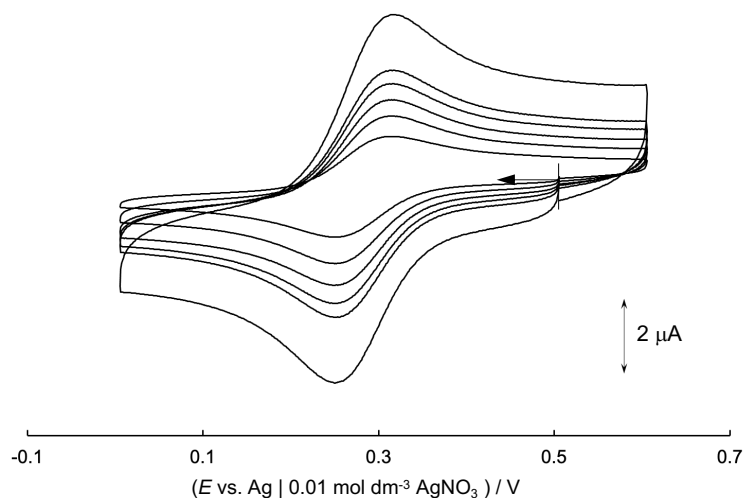


**Figure S9.** Cyclic voltammograms of the first reduction wave of  $[\text{IV},\text{IV}]^{2+}$  with the scan rate of 50, 100, 150, 200, 250, and  $500 \text{ mV s}^{-1}$ .

**Table S2.** Redox potentials of the first reduction wave of  $[\text{IV},\text{IV}]^{2+}$ .

scan rate / $\text{mV s}^{-1}$	$E_{\text{pc}} / \text{V}$	$E_{\text{pa}} / \text{V}$	$E_{1/2} / \text{V}$
50	0.17	0.11	0.14
100	0.17	0.12	0.15
150	0.17	0.12	0.15
200	0.18	0.12	0.15
250	0.18	0.11	0.15
500	0.18	0.11	0.15

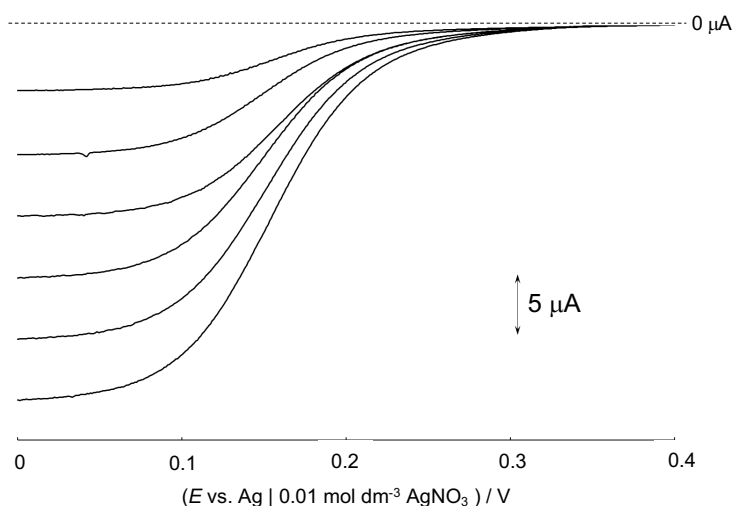


**Figure S10.** Hydrodynamic voltammograms of the first reduction wave of  $[\text{IV},\text{IV}]^{2+}$ .

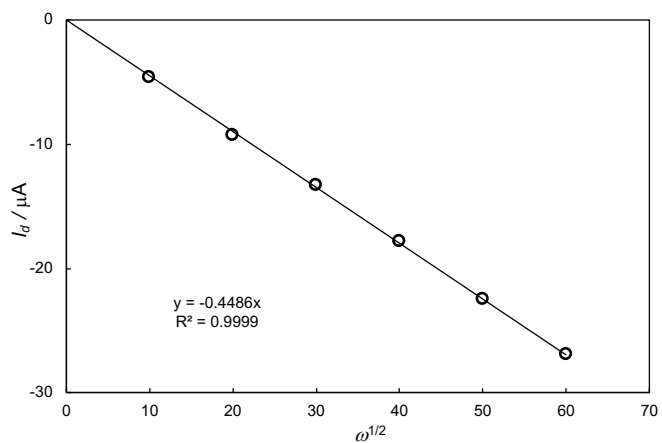


**Figure S11.** Analysis of the HDVs.

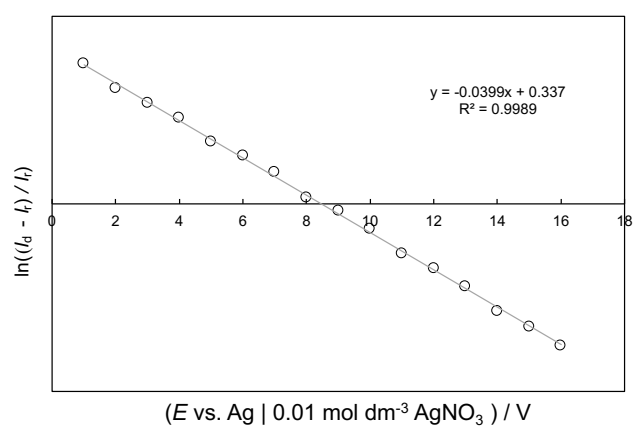


**Figure S12.** An ln-plot vs. redox potential.

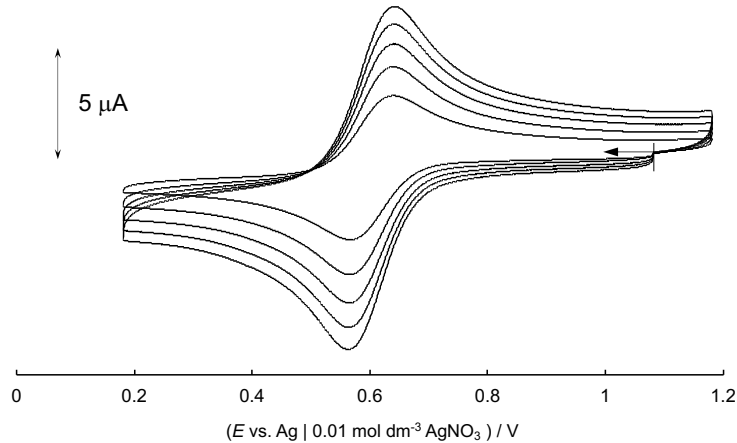


**Figure S13.** Cyclic voltammograms of the first reduction wave of  $[\text{IV},\text{IV}_1\text{H}]^{3+}$  with the scan rate of 50, 100, 150, 200, 250, and 500  $\text{mV s}^{-1}$ .

**Table S3.** Redox potentials of the first reduction wave of  $[\text{IV},\text{IV}_1\text{H}]^{3+}$ .

scan rate / $\text{mV s}^{-1}$	$E_{\text{pc}} / \text{V}$	$E_{\text{pa}} / \text{V}$	$E_{1/2} / \text{V}$
50	0.57	0.64	0.60
100	0.57	0.64	0.60
150	0.57	0.64	0.60
200	0.57	0.64	0.60
250	0.57	0.64	0.61

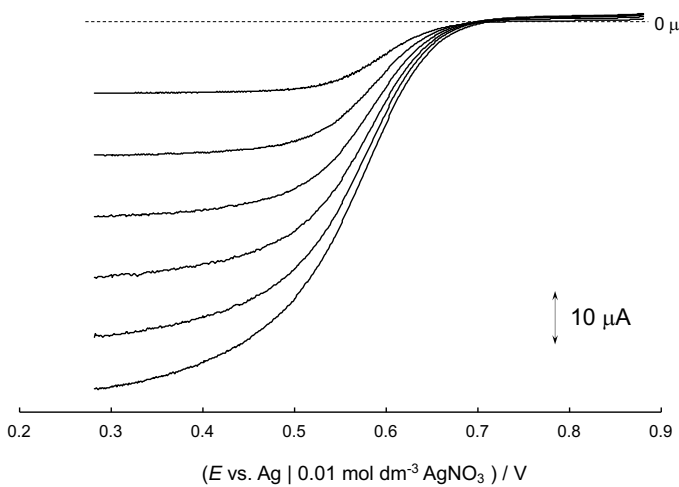


**Figure S14.** Hydrodynamic voltammograms of the first reduction wave of  $[IV,IV\_1H]^{3+}$ .

**Figure S15.** Analysis of the HDVs.

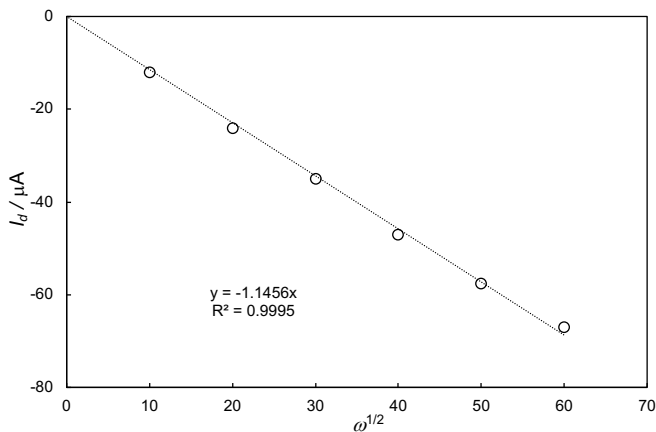


**Figure S16.** An ln-plot vs. redox potential.

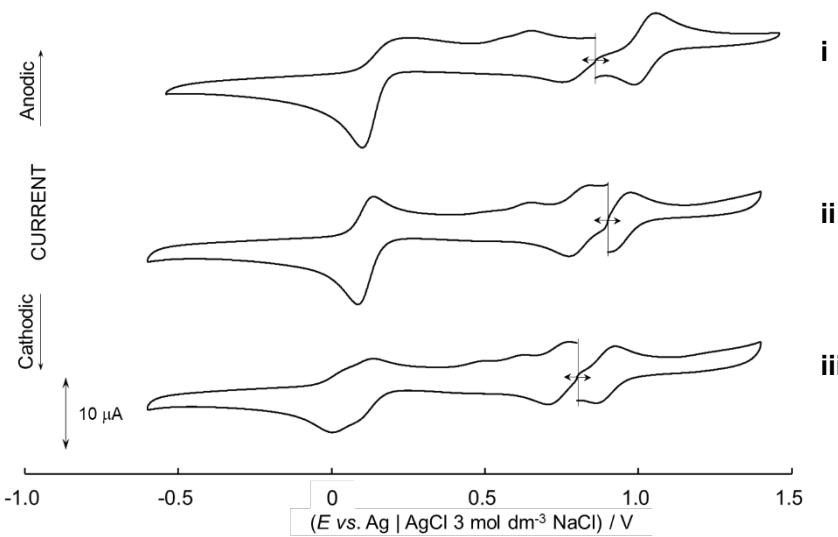
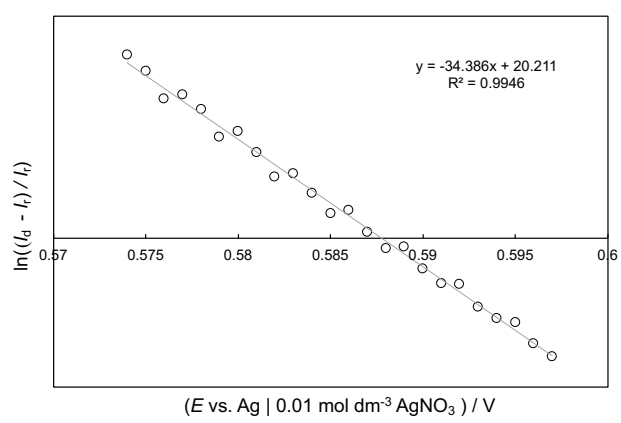


**Figure S17.** CVs of  $[III,IV]^{+}$  and  $[III,IV\_1H]^{2+}$  (1.3 mM) in  $HClO_4$  (aq.) –  $NaOH$  (aq.) / acetone ( $v/v = 9/1$ ); (i) pH 1.12, (ii) pH 1.75 and (iii) pH 2.73.

## II. X-ray crystallography

Single crystals were grown by a slow evaporation of a pH 3.5 solution of  $\text{Na}[\text{III},\text{IV}]_2(\text{ClO}_4)_3$ <sup>S4</sup> solution containing CAS for  $[\text{IV},\text{IV}](\text{ClO}_4)_2 \cdot 2\text{H}_2\text{O}$  and a pH 1.2  $\text{HClO}_4$  (aq.) solution for  $[\text{IV},\text{IV\_1H}](\text{ClO}_4)_3 \cdot \text{HClO}_4 \cdot \text{H}_2\text{O}$  at room temperature over a week. The intensity data were collected on a Rigaku Synergy-S, using multi-layer mirror monochromated  $\text{CuK}\alpha$  ( $1.54184 \text{ \AA}$ ) radiation. All the calculations were carried out using CrysAlis<sup>Pro</sup> (Data Collection and Processing Software, Rigaku Co. (2015)). Structures were solved by a direct method, expanded by Fourier techniques and refined using full-matrix least-squares techniques on  $F^2$  using SHELXT using Olex2 1.2.<sup>S5</sup>

**Table S4.** Crystallographic data.

	$[\text{IV},\text{IV}](\text{ClO}_4)_2 \cdot 2\text{H}_2\text{O}$	$[\text{IV},\text{IV\_1H}](\text{ClO}_4)_3 \cdot \text{HClO}_4 \cdot \text{H}_2\text{O}$
Formula	$\text{C}_{29}\text{H}_{34}\text{N}_6\text{O}_{15}\text{Cl}_2\text{Ru}_2$	$\text{C}_{29}\text{H}_{37}\text{N}_6\text{O}_{22}\text{Cl}_4\text{Ru}_2$
$F_w$	979.66	1165.58
Crystal size / mm	$0.067 \times 0.067 \times 0.030$	$0.10 \times 0.067 \times 0.067$
Crystal system	Triclinic	Triclinic
Space group	$P-1$ (#2)	$P-1$ (#2)
$a$ / $\text{\AA}$	12.1701(2)	12.58570(10)
$b$ / $\text{\AA}$	13.1905(2)	13.65550(10)
$c$ / $\text{\AA}$	13.4573(3)	13.97300(10)
$\alpha$ / $^\circ$	116.757(2)	79.7680(10)
$\beta$ / $^\circ$	91.744(1)	81.3400(10)
$\gamma$ / $^\circ$	98.840(1)	82.2290(10)
$V$ / $\text{\AA}^3$	1893.88(7)	2321.76(3)
$Z$	2	2
$D_{\text{calc}}$ / $\text{g cm}^{-3}$	1.718	1.667
$\mu(\text{CuK}\alpha)$ / $\text{mm}^{-1}$	8.417	8.125
$T$ / $^\circ\text{C}$	25	25
No. of observed refln.	21288	27538
No. of variables	7562	9278
$R^{\text{a})}$ / $wR^{\text{b})}$	0.0404 / 0.1153	0.0395 / 0.1134
$R_{\text{int}}$	0.0375	0.0362
GOF	1.071	1.026

a)  $R = \Sigma |F_{\text{o}}| - |F_{\text{c}}| / \Sigma |F_{\text{o}}|$  ( $I > 2\sigma(I)$ ), b)  $wR = [\Sigma (w(F_{\text{o}}^2 - F_{\text{c}}^2)^2 / \Sigma w(F_{\text{o}}^2)_2)]^{1/2}$  (all reflections)

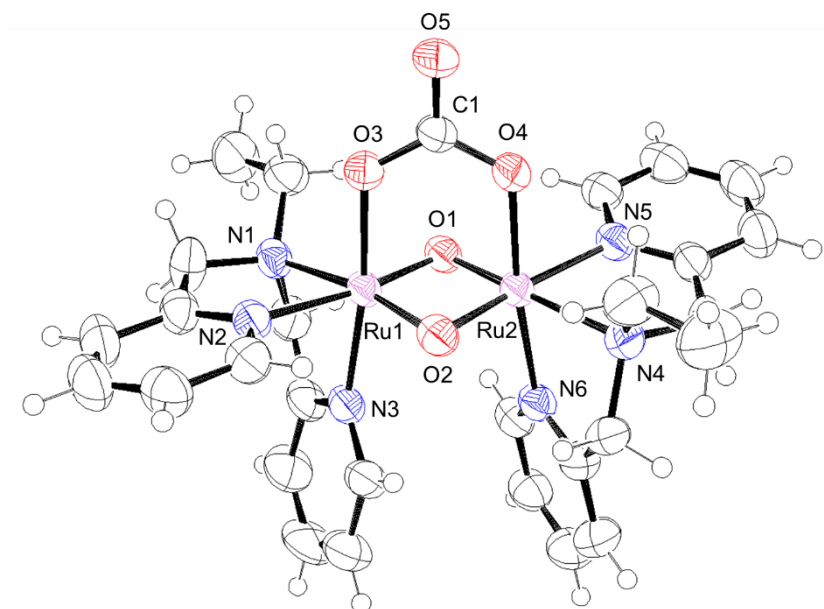


**Figure S18.** Structure of  $[IV,IV]^{2+}$  shown at the 50 % thermal ellipsoid probability level.

**Table S5.** Selected structural parameters of **[IV,IV](ClO<sub>4</sub>)<sub>2</sub>·2H<sub>2</sub>O** and **[IV,IV\_1H](ClO<sub>4</sub>)<sub>3</sub>·HClO<sub>4</sub>·H<sub>2</sub>O**.

	<b>[IV,IV](ClO<sub>4</sub>)<sub>2</sub>·2H<sub>2</sub>O</b>		<b>[IV,IV_1H](ClO<sub>4</sub>)<sub>3</sub>·HClO<sub>4</sub>·H<sub>2</sub>O</b>		<b>K[III,IV]<sub>2</sub>(PF<sub>6</sub>)<sub>3</sub>·3CH<sub>3</sub>CN·4H<sub>2</sub>O<sup>S4</sup></b>		<b>[III,IV_1H](ClO<sub>4</sub>)<sub>2</sub>·H<sub>2</sub>O<sup>S4</sup></b>		<b>Na[III,IV_2H](ClO<sub>4</sub>)<sub>4</sub>·4H<sub>2</sub>O<sup>S4</sup></b>	
<b>Bond distances / Å</b>										
Ru1,2-O1	1.905(3)	1.914(3)	1.918(2)	1.899(2)	1.940(5)	1.940(4)	1.9372(18)	1.9329(17)	1.954(4)	1.953(4)
Ru1,2-O2	1.904(3)	1.919(3)	1.902(2)	1.914(2)	1.938(4)	1.962(5)	1.9360(18)	1.9387(18)	2.022(4)	2.019(3)
Ru1---Ru2	2.4261(3)		2.4389(3)		2.4434(8)		2.4547(2)		2.5332(5)	
Ru-O3,4	2.031(3)	2.022(3)	2.069(2)	2.065(2)	2.055(4)	2.063(4)	2.0799(17)	2.0968(18)	2.078(4)	2.083(4)
Ru-N1,4	2.147(3)	2.146(3)	2.130(3)	2.134(3)	2.195(5)	2.168(5)	2.158(2)	2.156(2)	2.131(4)	2.123(4)
Ru-N2,5	2.091(3)	2.091(3)	2.078(3)	2.086(3)	2.113(7)	2.100(6)	2.087(2)	2.093(2)	2.072(3)	2.088(4)
Ru-N3,6	2.076(3)	2.072(3)	2.047(3)	2.056(3)	2.061(5)	2.057(5)	2.039(2)	2.042(2)	2.042(5)	2.045(5)
O3,4-C29	1.311(5)	1.312(4)	1.265(4)	1.269(4)	1.309(8)	1.301(8)	1.258(3)	1.266(3)	1.266(7)	1.266(6)
C29-O5	1.228(5)		1.297(4)		1.252(7)		1.315(3)		1.313(7)	
<b>Bond angles / °</b>										
Ru1-O1,2-Ru2	79.14(10)	78.53(10)	79.34(9)	79.53(8)	78.06(17)	77.60(17)	78.66(7)	78.69(7)	O1; 77.65(13) O2; 80.82(16)	
O1-Ru1,2-O2	101.09(11)	100.93(11)	100.45(9)	100.47(9)	102.6(2)	101.7(2)	101.34(7)	101.17(7)	100.50(15)	100.67(15)
O2,1-Ru-N1,4	167.12(13)	170.19(11)	167.97(11)	169.15(11)	168.3(2)	168.5(2)	166.15(19)	168.5(2)	167.39(18)	171.40(16)
O1,2-Ru-N1,4	89.56(13)	91.59(13)	91.00(11)	90.51(11)	86.4(2)	88.0(2)	86.4(2)	88.0(2)	89.93(16)	91.54(16)
O1,2-Ru-N2,5	168.76(13)	167.47(13)	167.97(11)	168.23(11)	166.15(19)	168.03(18)	166.15(19)	168.03(18)	169.58(15)	167.77(17)
O1-Ru-N3,6	93.07(13)	95.53(12)	94.30(11)	95.07(11)	90.10(19)	97.4(2)	98.7(2)	90.1(2)	93.49(18)	95.09(19)
O2-Ru-N3,6	94.56(12)	92.23(13)	94.83(11)	94.29(11)	98.7(2)	91.05(18)	90.10(19)	97.4(2)	92.74(18)	93.09(18)
Ru1,2-O3,4-C29	122.0(2)	121.2(2)	119.8(2)	120.2(2)	78.06(17)	77.60(17)	119.41(16)	119.95(16)	120.9(3)	120.4(4)
O3-C29-O4	120.8(3)		125.2(3)		120.5(5)		126.0(2)		126.2(5)	
O3-C29-O5	119.4(3)	119.8(3)	119.0(3)	115.8(3)	118.9(6)	120.6(6)	118.5(2)	115.6(2)	115.1(5)	118.7(5)

### III. UV-vis-NIR spectra in various organic solvents at 298 K

#### *A Reaction in DMSO.*

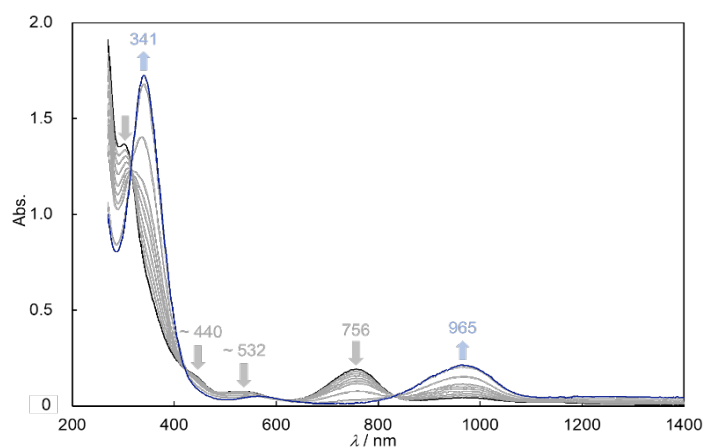


**Figure S19.** Spectral changes in a reaction of  $[\text{IV},\text{IV}_1\text{H}]^{3+}$  in dehydrated DMSO.

#### *A Reaction in nitromethane.*

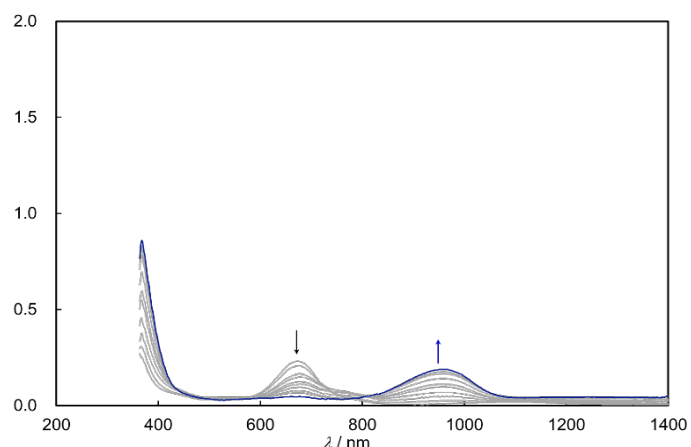


**Figure S20.** Spectral changes in a reaction of  $[\text{IV},\text{IV}_1\text{H}]^{3+}$  in dehydrated nitromethane

#### *Authentic spectra of Ru(III)-Ru(IV) complexes*

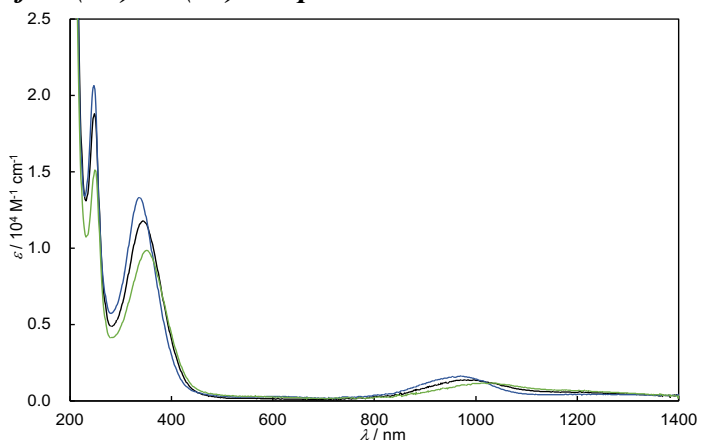


**Figure S21.** Authentic spectra of  $[\text{III},\text{IV}]^+$  (yellow green line),  $[\text{III},\text{IV}_1\text{H}]^{2+}$  (black line) and  $[\text{III},\text{IV}_2\text{H}]^{3+}$  (blue line) in dehydrated methanol.

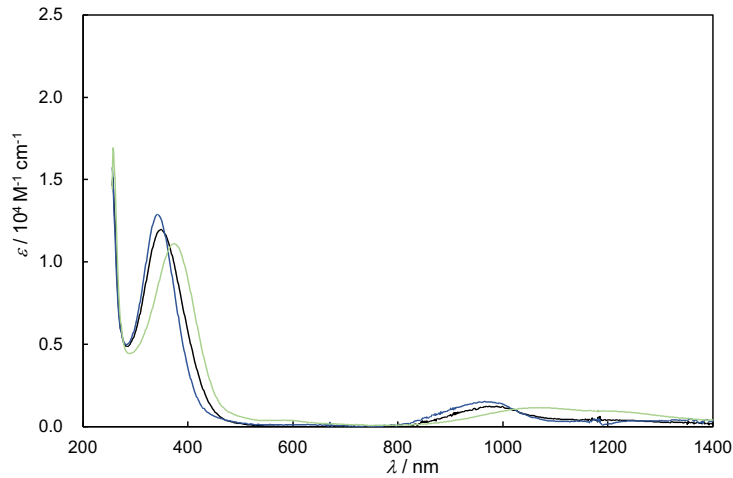


**Figure S22.** Authentic spectra of  $[\text{III},\text{IV}]^{2+}$  (yellow green line),  $[\text{III},\text{IV}_1\text{H}]^{2+}$  (black line) and  $[\text{III},\text{IV}_2\text{H}]^{3+}$  (blue line) in dehydrated DMSO.

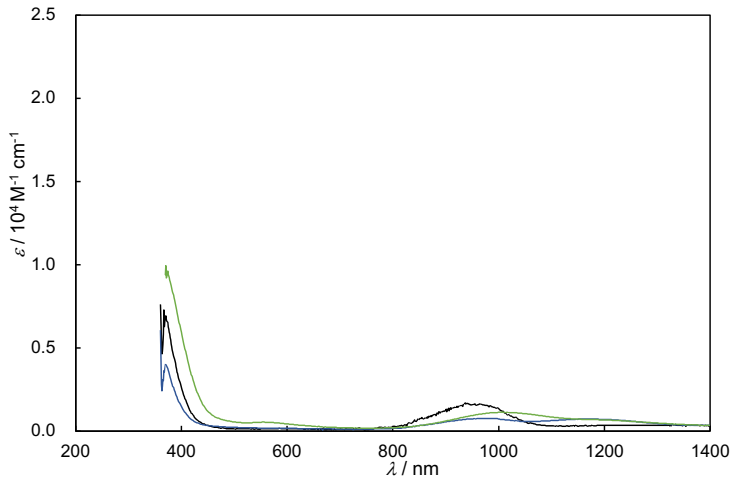


**Figure S23.** Authentic spectra of  $[\text{III},\text{IV}]^{2+}$  (yellow green line),  $[\text{III},\text{IV}_1\text{H}]^{2+}$  (black line) and  $[\text{III},\text{IV}_2\text{H}]^{3+}$  (blue line) in nitromethane.

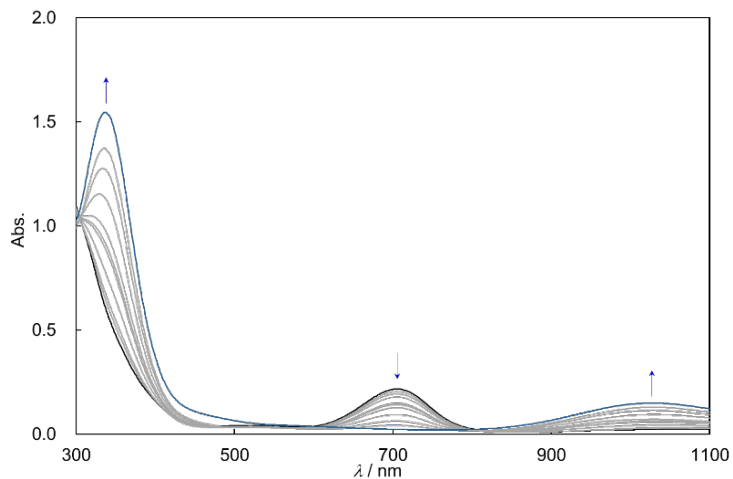


**Figure S24.** Spectral changes of  $[\text{IV},\text{IV}]^{2+}$  in a pH 4 water.

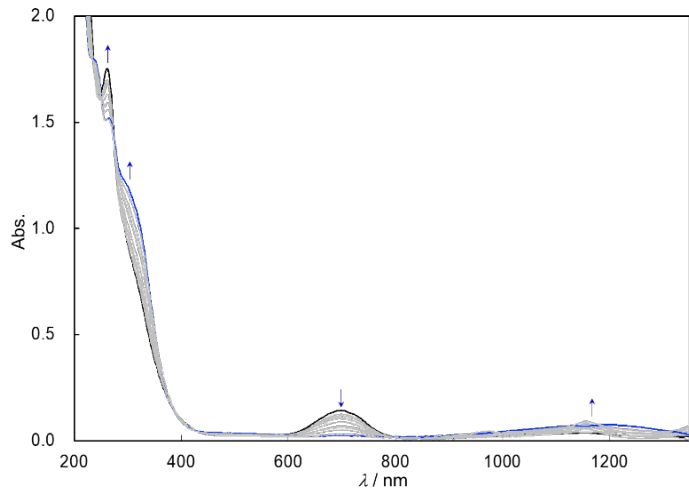


**Figure S25.** Spectral changes of  $[IV,IV\_1H]^{3+}$  in a pH 1 water.

**Reactions in acetone.**

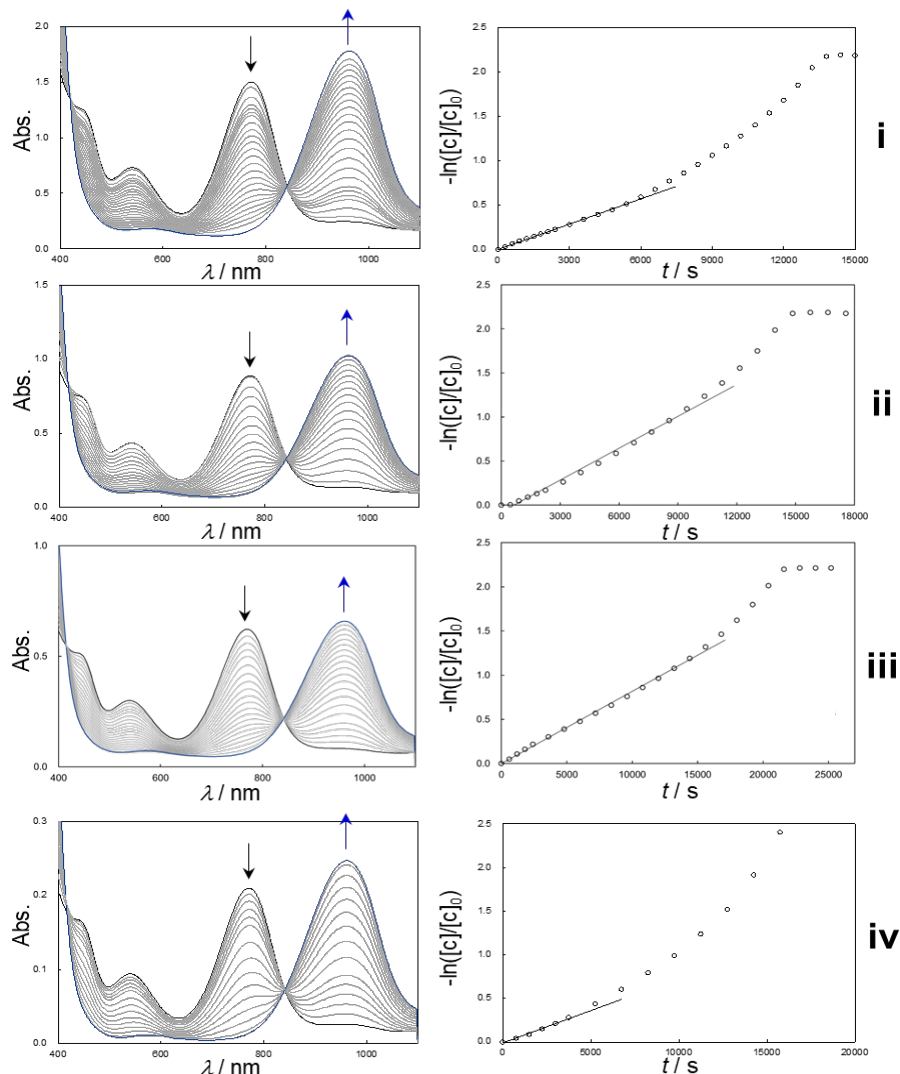


**Figure S26.** Spectral changes in reactions of  $[IV,IV]^{2+}$  in acetone; i) 1.0 mM, ii) 0.65 mM, iii) 0.40 mM and iv) 0.20 mM;  $k, 10^{-5} \text{ s}^{-1} =$  i) 9.5, ii) 12.0, iii) 8.2 and iv) 7.5.

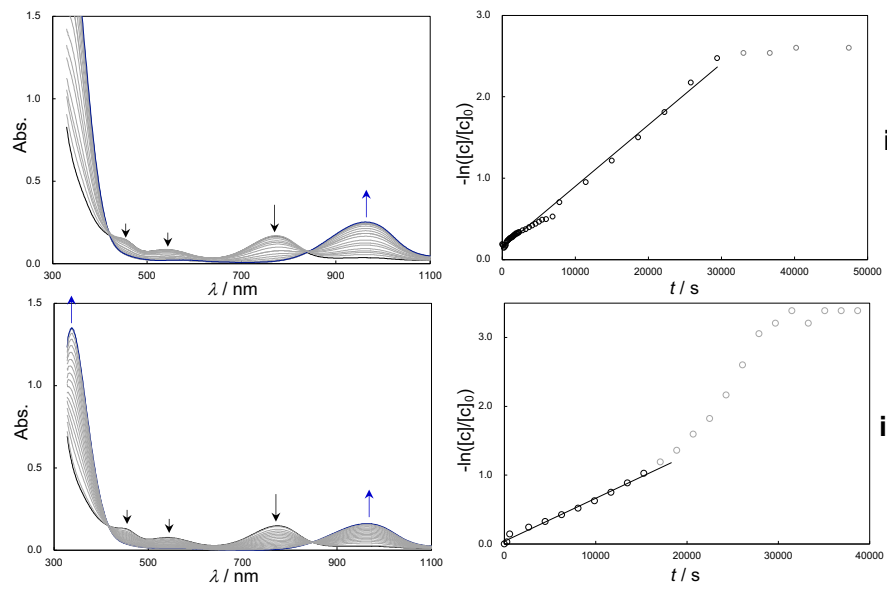


**Figure S27.** Spectral changes in reactions of  $[\text{IV},\text{IV}]^{2+}$  (0.14 mM) **i)** in acetone and **ii)** in super dehydrated acetone.  $k, 10^{-5} \text{ s}^{-1} = \text{i)} 7.5$  and **ii)** 6.2.

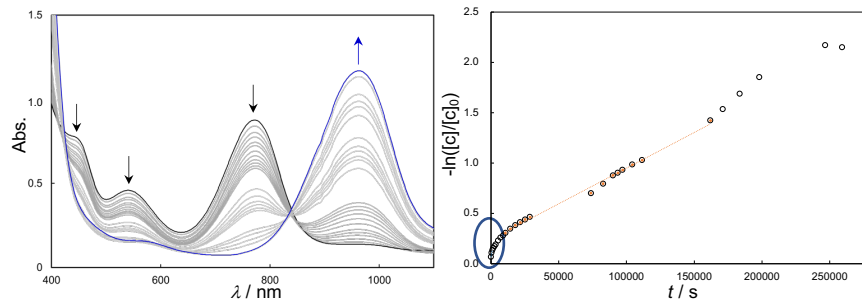


**Figure S28.** Spectral changes in reactions of  $[\text{IV},\text{IV}]^{2+}$  (0.65 mM) in acetone- $d_6$ .  $k, 10^{-5} \text{ s}^{-1} = 5.7$  (initial in blue), 0.71 (following in orange). KIE was calculated by using the initial rate.

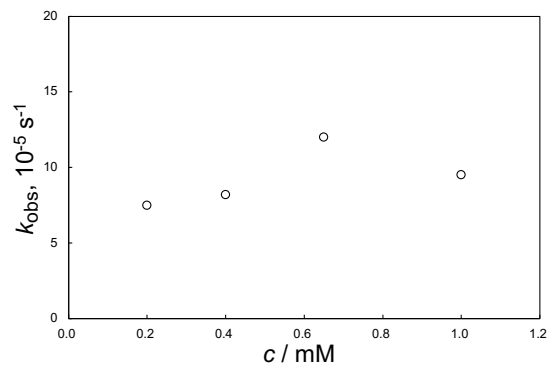


**Figure S29.**  $k_{\text{obs}}, 10^{-5} \text{ s}^{-1}$  vs. concentration of  $[\text{IV},\text{IV}]^{2+}$  for the reactions in acetone.

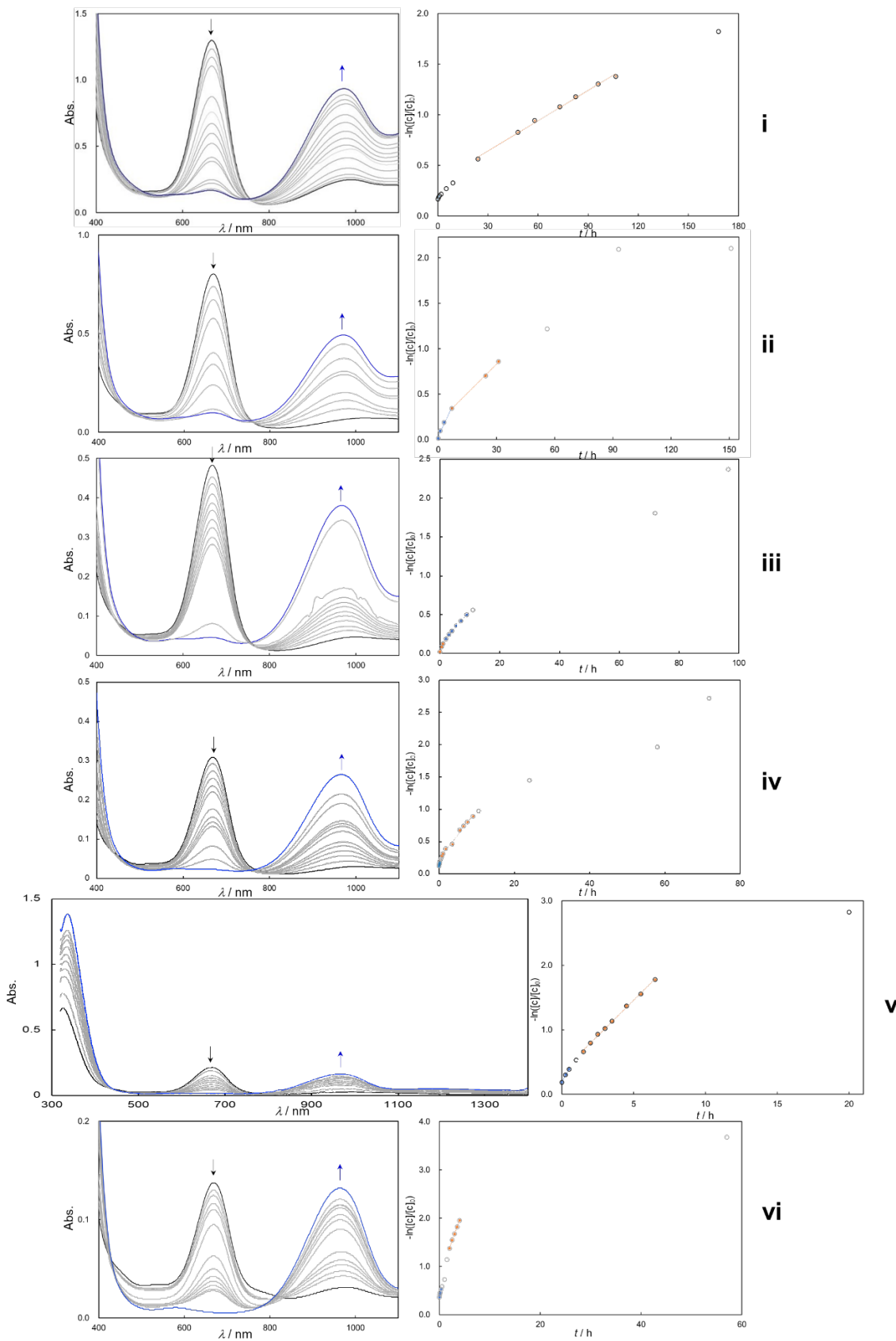


**Figure S30.** Spectral changes in reactions of  $[IV, IV\_1H]^{3+}$  in acetone; **i)** 0.78 mM, **ii)** 0.40 mM, **iii)** 0.25 mM, **iv)** 0.18 mM, **vi)** 0.13 mM, and **vii)** 0.10 mM.  $k, 10^{-2} \text{ h}^{-1}$  (initial, following) = **i)** 3.4, 0.99, **ii)** 4.5, 2.1, **iii)** 10.3, 4.4, **iv)** 31.9, 7.5, **v)** 40.7, 22.0 and **vi)** 49.5, 28.6.

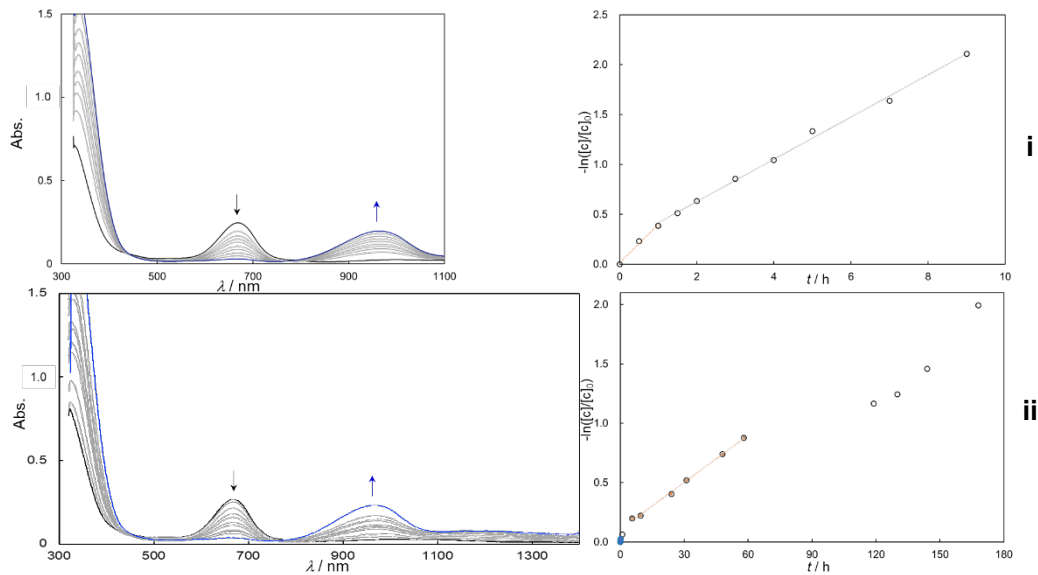


**Figure S31.** Spectral changes in reactions of  $[\text{IV},\text{IV-1H}]^{3+}$  (0.13 mM) in **i**) super dehydrated acetone-D<sub>2</sub>O ( $v/v = 99.5/0.5$ ) and **ii**) super dehydrated acetone.  $k, 10^{-2} \text{ h}^{-1}$  (initial, following) = **i**) 38.5, 21.2 and **ii**) 14.3, 1.3.

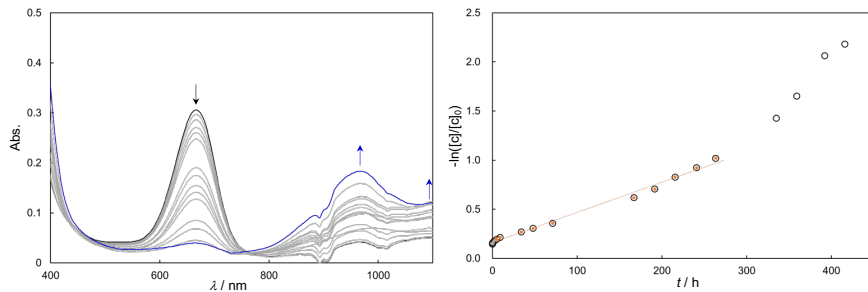


**Figure S32.** Spectral changes in reactions of  $[\text{IV},\text{IV-1H}]^{3+}$  (0.18 mM) in acetone-*d*<sub>6</sub>.  $k, 10^{-2} \text{ h}^{-1}$  (initial, following) = 1.3, 0.31.

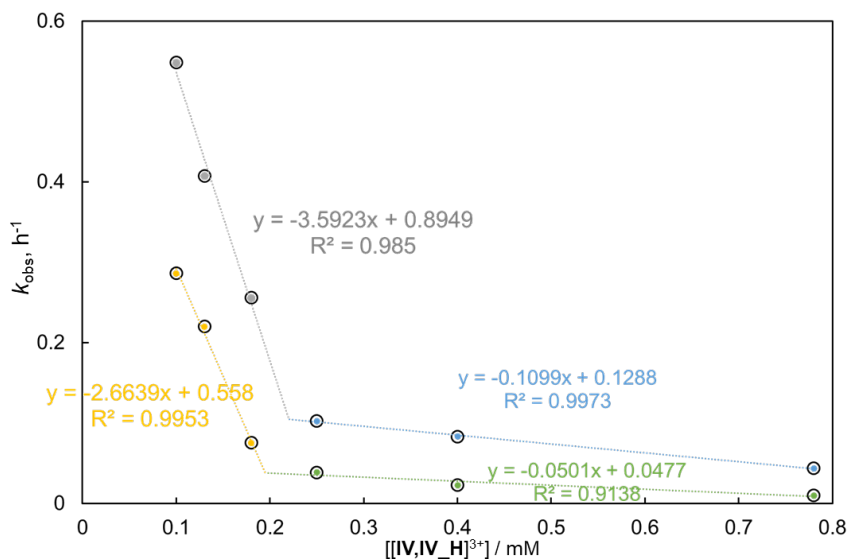


**Figure S33.** Dependency of concentration of  $[\text{IVIV-1H}]^{3+}$  in acetone.

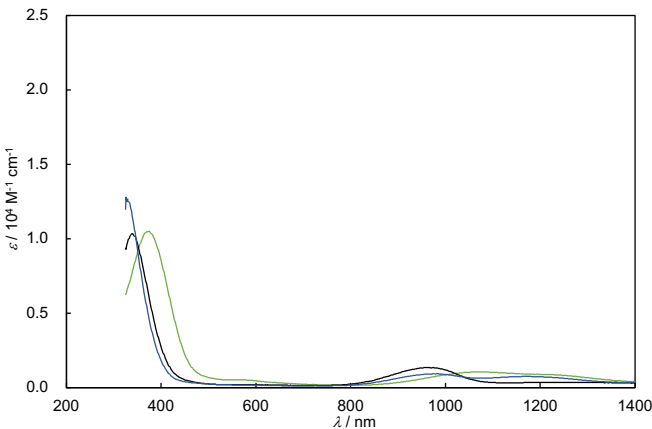


**Figure S34.** Authentic spectra of  $[III,IV]^{2+}$  (yellow green line),  $[III,IV\_1H]^{2+}$  (black line) and  $[III,IV\_2H]^{3+}$  (blue line) in dehydrated acetone.

### Reactions in acetonitrile

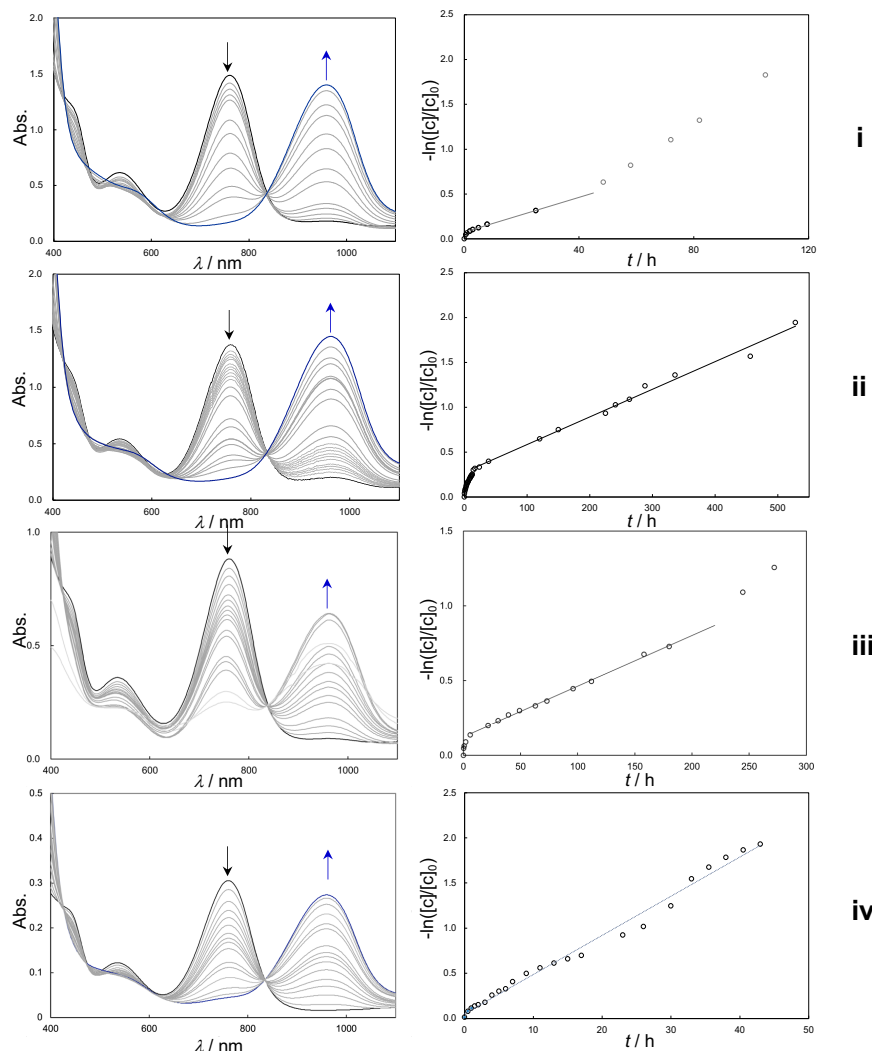


**Figure S35.** Spectral changes in reactions of  $[IV,IV]^{2+}$  in acetonitrile; **i)** 1.0 mM, **ii)** 0.82 mM, **iii)** 0.40 mM and **iv)** 0.20 mM.  $k, 10^{-2} \text{ h}^{-1}$  (initial, following) = **i)** 6.5, 0.97, **ii)** 2.5, 0.31, **iii)** 9.3, 0.34 and **iv)** 10, 0.43.

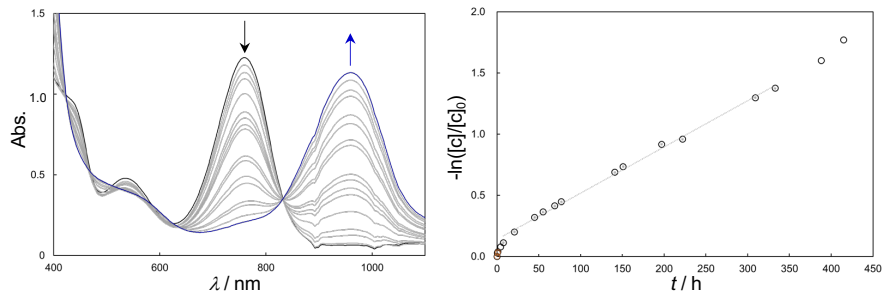


**Figure S36.** Spectral changes in reactions of  $[IV,IV]^{2+}$  (0.82 mM) in acetonitrile- $d_3$ .  $k, 10^{-2} \text{ h}^{-1}$  (initial, following) = 3.8, 0.38.

**Table S6.** Kinetic analyses of the reactions in aliphatic solvents with the methyl group(s) at 298 K.

solvent	$BDE_{C-H}$ kcal mol <sup>-1</sup> S6)	Reactions rate constant $k, \text{h}^{-1}$		KIE	
		$[IV,IV]^{2+}$	$[IV,IV\_1H]^{3+}$	$[IV,IV]^{2+}$	$[IV,IV\_1H]^{3+}$
DMSO (dehydrated)	94	$[IV,IV\_1H]^{3+}$ was changed into $[IV,IV]^{2+}$ upon dissolution, then, $[IV,IV]^{2+}$ was changed into $[III,IV\_2H]^{3+}$			
acetone	96.0	$< 0.2 \text{ mM};$ changed into $[III,IV\_2H]^{3+}$	$> 0.2 \text{ mM};$ changed into $[III,IV\_1H]^{2+}$	5.1 (0.65 mM)	2.2, 24 (0.18 mM)
methanol (dehydrated)	96.06	$[IV,IV\_1H]^{3+}$ was changed to $[IV,IV]^{2+}$ upon dissolution, then, $[IV,IV]^{2+}$ was changed into $[III,IV\_2H]^{3+}$			
acetonitrile	97.0	-	slowly changed into $[III,IV\_2H]^{3+}$	1.5, 1.2 (0.80 mM)	-
nitromethane (dehydrated)	99.3	-	slowly changed into $[III,IV\_1H]^{2+}$		-

#### IV. Spectroscopic studies on oxidation of C-H bond of ring organic compounds

*Reactions with benzyl alcohol (BA) in dehydrated acetonitrile.*

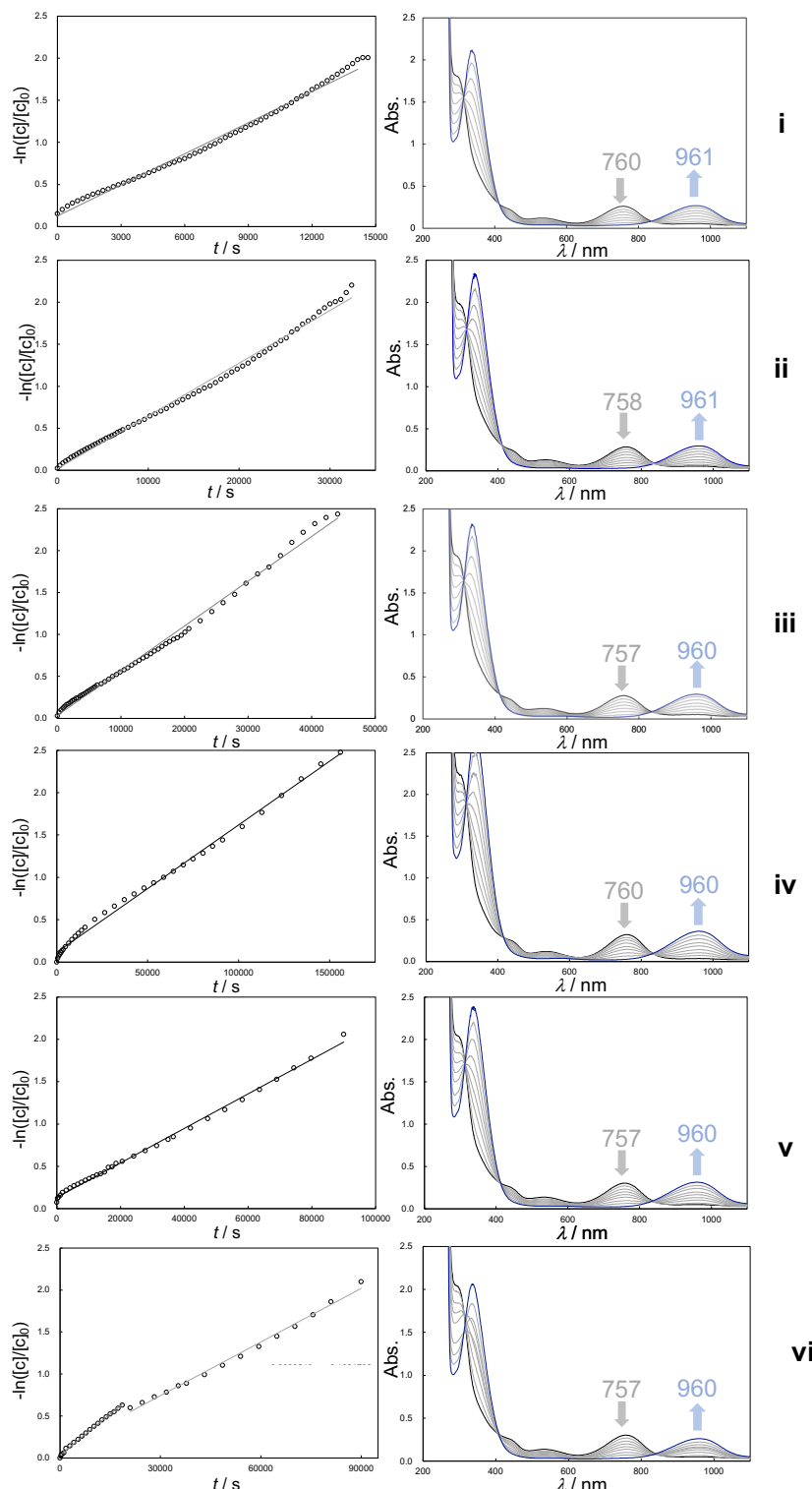


**Figure S37.** Spectral changes in reactions of  $[IV, IV]^{2+}$  (0.20 mM) with benzyl alcohol; **i)** 0.2 M, **ii)** 0.176 M, **iii)** 0.15 M, **iv)** 0.15 M- $d_2$ , **v)** 0.1 M and **vi)** 0.05 M.  $k, 10^{-5} \text{ s}^{-1} =$  **i)** 12.3, **ii)** 6.3, **iii)** 5.3, **iv)** 2.0 and **v)** 2.1.

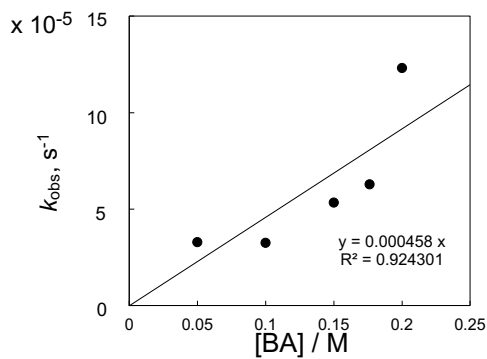


**Figure S38.** A plot of  $k_{\text{obs}}$ ,  $10^{-5} \text{ s}^{-1}$  vs. concentration of benzyl alcohol  $[\text{BA}] / \text{M}$  in reactions of  $[\text{IV}, \text{IV}]^{2+}$ .  $k'$ ,  $\text{M}^{-1} \text{ s}^{-1} = k/2 = 2.3 \times 10^{-4}$ .

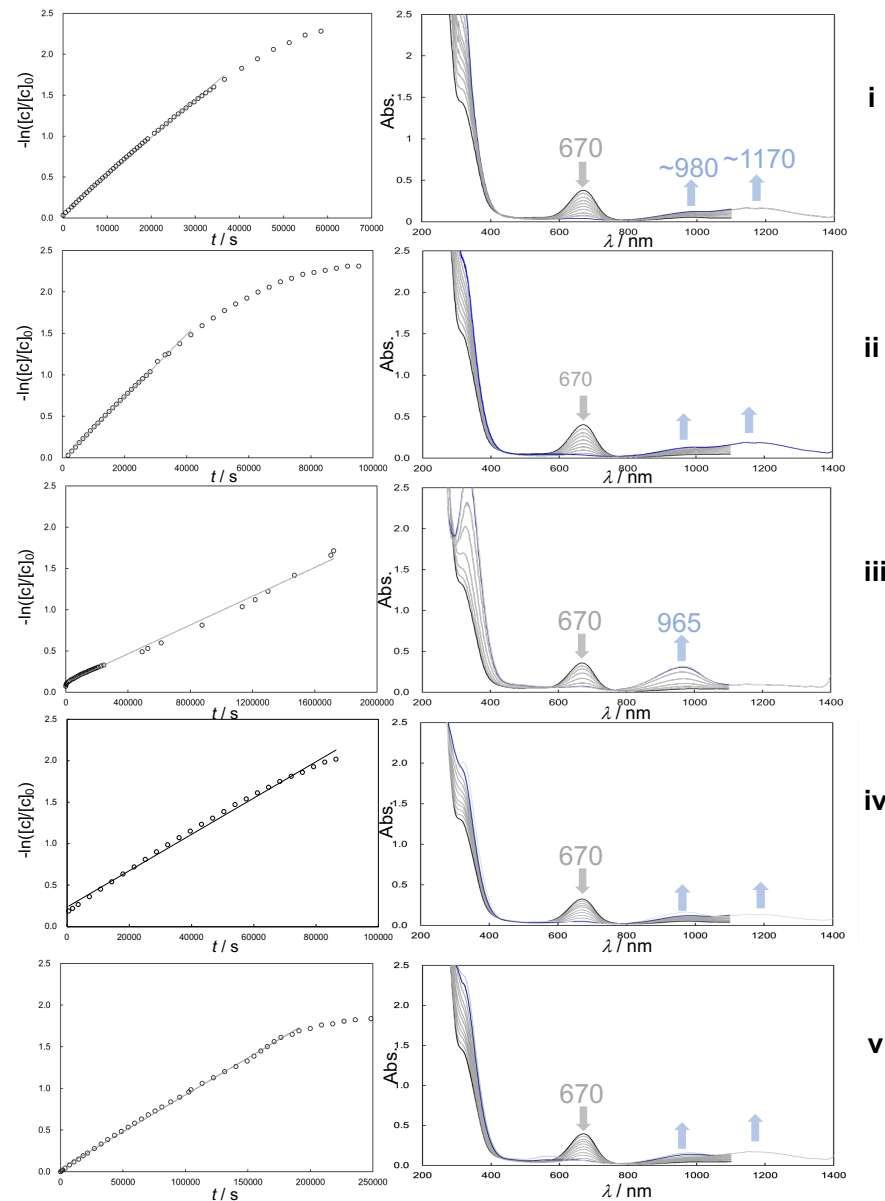


**Figure S39.** Spectral changes in reactions of  $[\text{IV}, \text{IV-1H}]^{3+}$  (0.20 mM) with benzyl alcohol; **i)** 0.2 M, **ii)** 0.15 M, **iii)** 0.15 M- $d_2$ , **iv)** 0.1 M and **v)** 0.05 M.  $k$ ,  $10^{-5} \text{ s}^{-1}$  = **i)** 4.6, **ii)** 3.8, **iii)** 0.087, **iv)** 2.2 and **v)** 0.89.

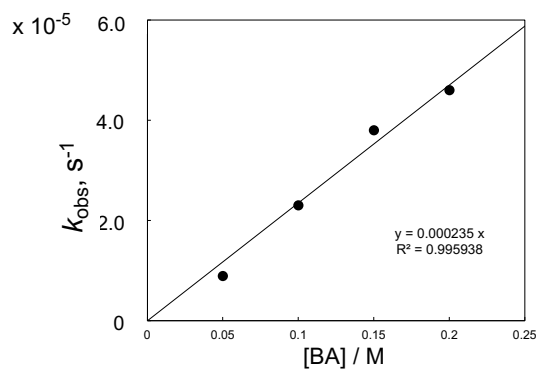


**Figure S40.** A plot of  $k_{\text{obs}}$  against concentration of benzyl alcohol [BA] / M in reactions of  $[\text{IV}, \text{IV}_1\text{H}]^{3+}$ .  $k'$ ,  $\text{M}^{-1} \text{s}^{-1} = k/2 = 1.2 \times 10^{-4}$ .

**Reactions with cyclohexene in dehydrated acetonitrile.**

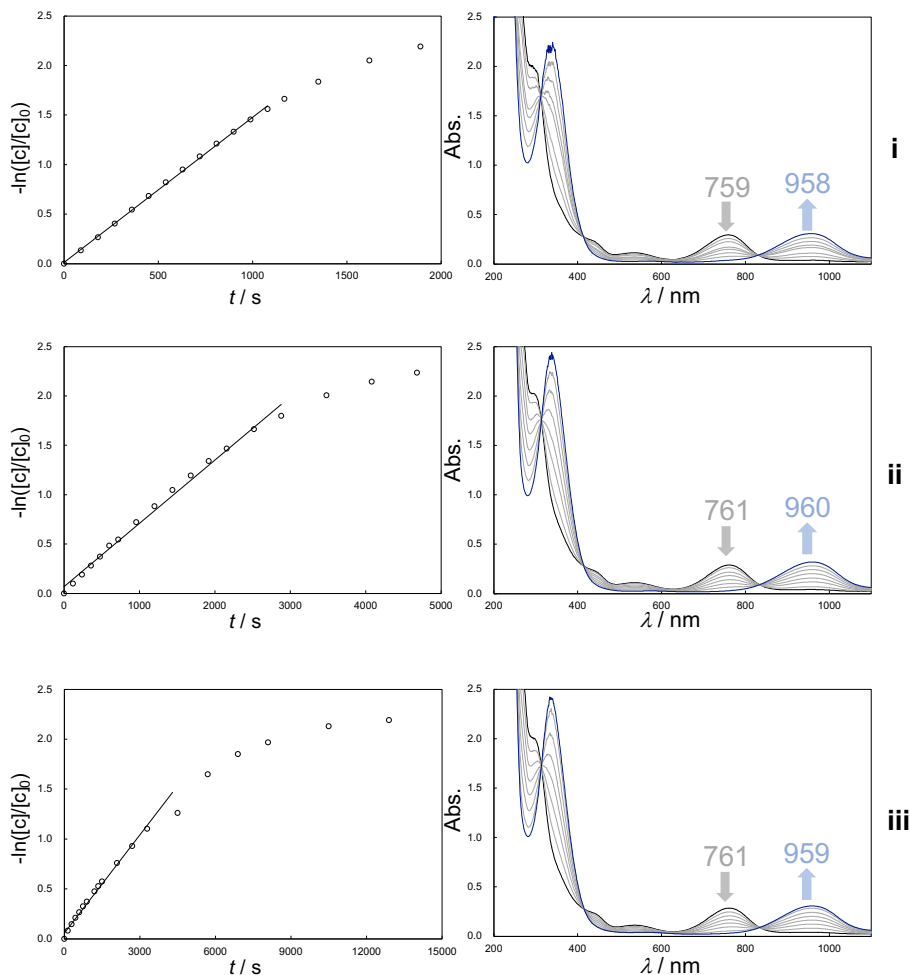


**Figure S41.** Spectral changes in reactions of  $[\text{IV}, \text{IV}]^{2+}$  (0.20 mM) with cyclohexene; **i**) 0.2 M, **ii**) 0.1 M and **iii**) 0.05 M.  $k, 10^{-3} \text{s}^{-1} = \mathbf{i}) 1.5, \mathbf{ii}) 0.64$  and **iii**) 0.33.

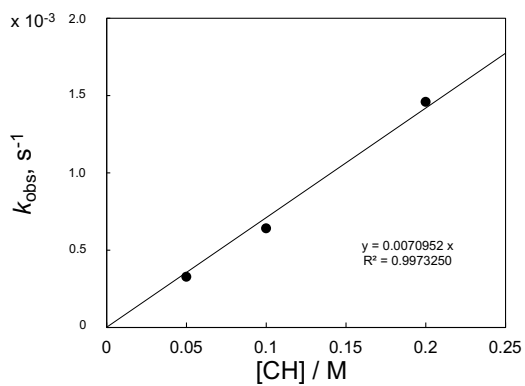


**Figure S42.** A plot of  $k_{\text{obs}}$ ,  $10^{-3}$   $\text{s}^{-1}$  against concentration of cyclohexene  $[\text{CH}] / \text{M}$  in reactions of  $[\text{IV},\text{IV}]^{2+}$ .  $k' = k/4 = 1.8 \times 10^{-3}$ .

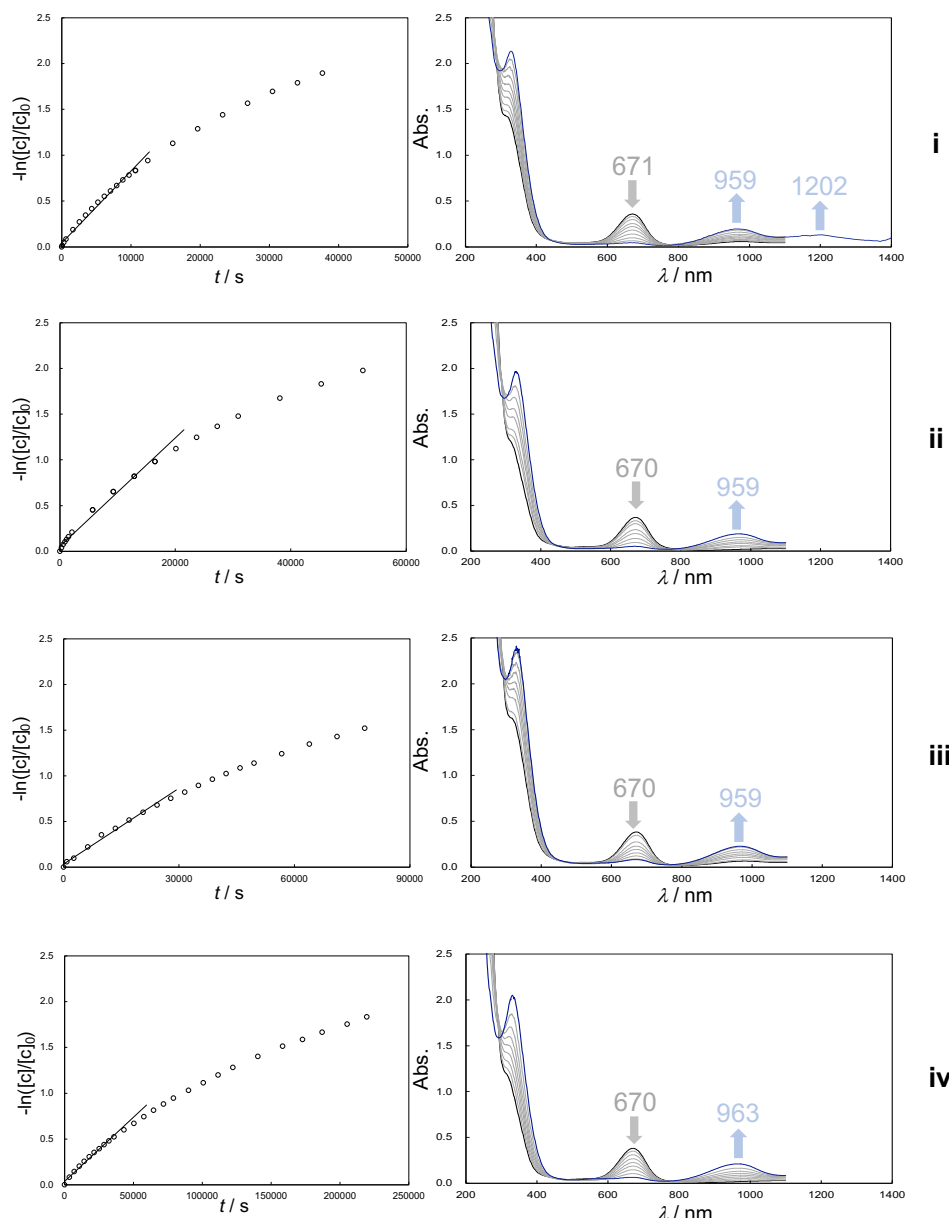


**Figure S43.** Spectral changes in reactions of  $[\text{IV},\text{IV}_1\text{H}]^{3+}$  (0.20 mM) with cyclohexene; **i)** 0.2 M, **ii)** 0.15 M, **iii)** 0.1 M and **iv)** 0.05 M.  $k, 10^{-5} \text{ s}^{-1} = \text{i}) 7.8, \text{ii}) 5.9, \text{iii}) 2.8$  and **iv)** 1.4.

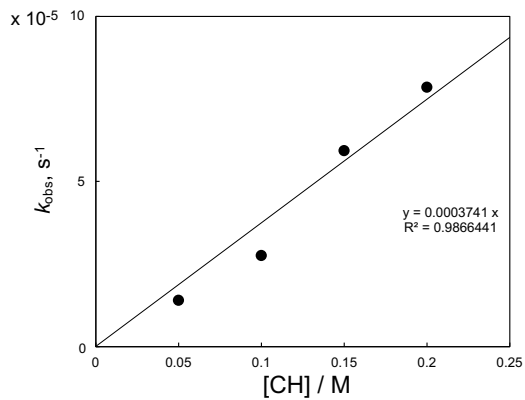


**Figure S44.** A plot of  $k_{\text{obs}}$ ,  $10^{-5} \text{ s}^{-1}$  against concentration of cyclohexene  $[\text{CH}] / \text{M}$  in reactions of  $[\text{IV}, \text{IV}_1\text{H}]^{3+} \cdot K'$ ,  $\text{M}^{-1} \text{ s}^{-1} = k/4 = 9.4 \times 10^{-5}$ .

#### Reactions with cumene in dehydrated acetonitrile.

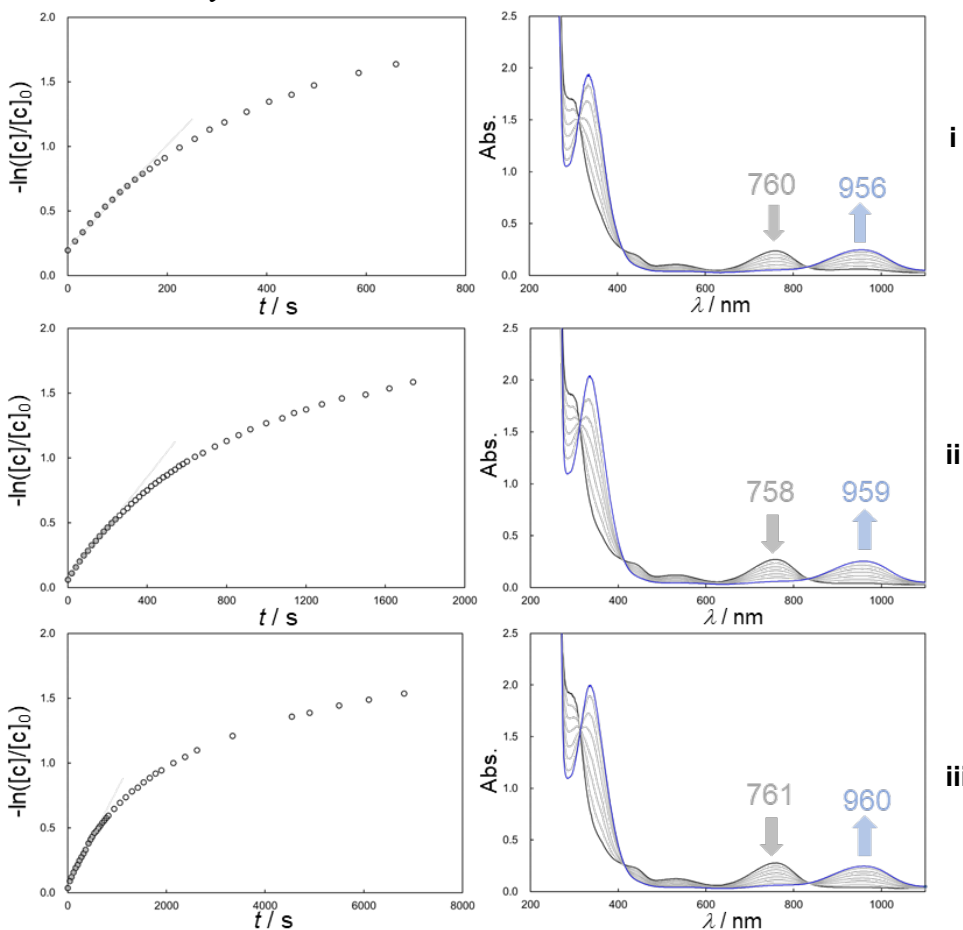


**Figure S45.** Spectral changes in reactions of  $[\text{IV}, \text{IV}]^{2+}$  (0.20 mM) with cumene; **i)** 0.2 M, **ii)** 0.1 M and **iii)** 0.05 M.  $k = 10^{-3} \text{ s}^{-1}$  = **i)** 4.0, **ii)** 1.9 and **iii)** 0.73.

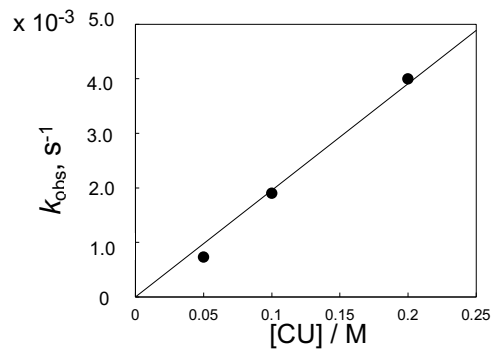


**Figure S46.** A plot of  $k_{\text{obs}}$ ,  $10^{-3}$   $\text{s}^{-1}$  against concentration of cumene  $[\text{CU}] / \text{M}$  in reactions of  $[\text{IV,IV}]^{2+}$ .

$$k', \text{M}^{-1} \text{s}^{-1} = 2.0 \times 10^{-2}$$

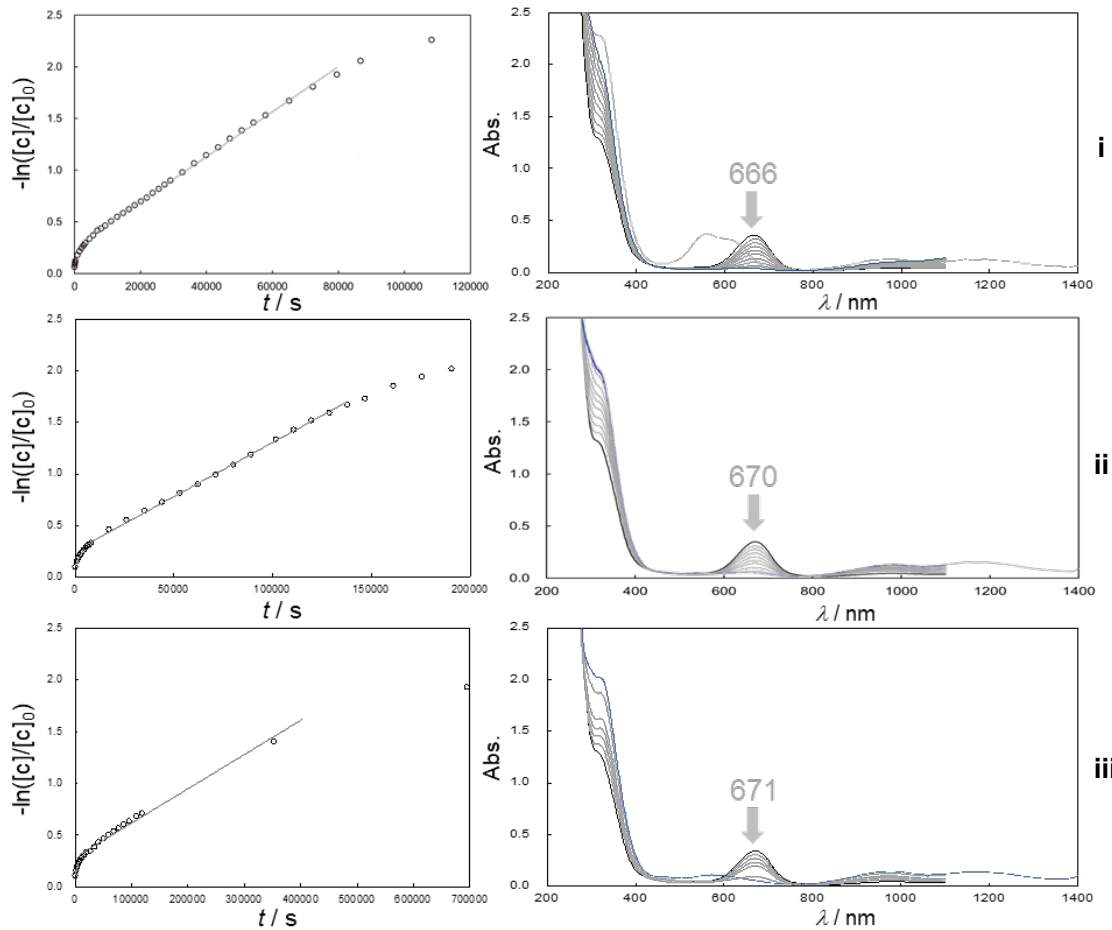


**Figure S47.** Spectral changes in reactions of  $[\text{IV,IV}_1\text{H}]^{3+}$  (0.20 mM) with cumene; **a)** 0.2 M, **b)** 0.1 M and **c)** 0.05 M.  $k$ ,  $10^{-5}$   $\text{s}^{-1}$  (initial, following) = **i)** 7.4, 2.2, **ii)** 3.6, 1.1 and **iii)** 1.8, 0.33.

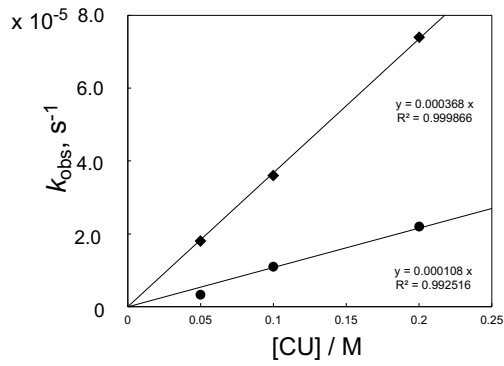


**Figure S48.** A plot of  $k_{\text{obs}}$ ,  $10^{-5} \text{ s}^{-1}$  against concentration of cumene  $[\text{CU}] / \text{M}$  in reactions of  $[\text{IV}, \text{IV\_1H}]^{3+}$ ;  $\blacklozenge$  initial reaction,  $\bullet$  following reaction.  $k'$ ,  $\text{M}^{-1} \text{ s}^{-1} = 3.7 \times 10^{-4}$ ,  $1.1 \times 10^{-4}$ .

**Reactions with ethylbenzene in dehydrated acetonitrile.**

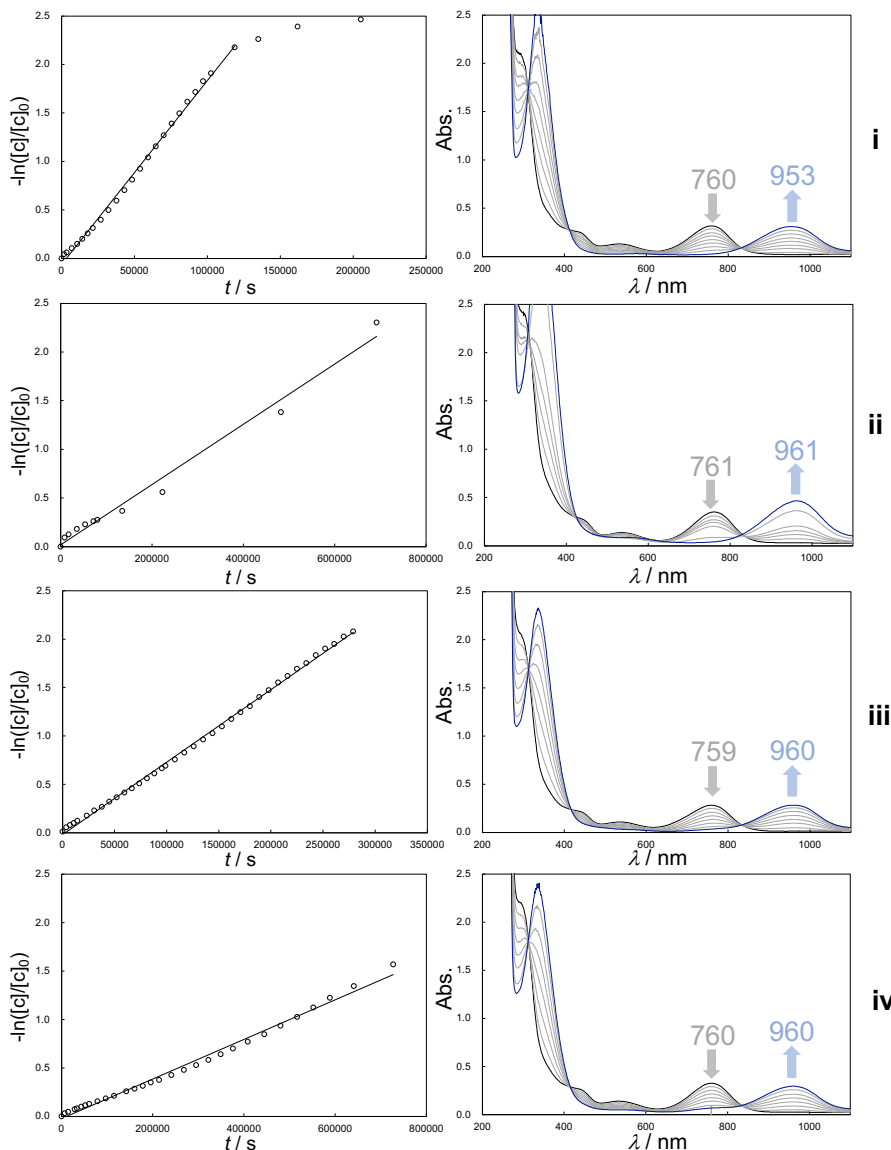


**Figure S49.** Spectral changes in reactions of  $[\text{IV}, \text{IV}]^+$  ( $0.2 \text{ mM}$ ) with ethylbenzene; **i)**  $0.2 \text{ M}$ , **ii)**  $0.2 \text{ M-EB-}d_{10}$ , **iii)**  $0.10 \text{ M}$  and **iv)**  $0.05 \text{ M}$ .  $k$ ,  $10^{-5} \text{ s}^{-1} = \mathbf{i)} 1.9$ ,  $\mathbf{ii)} 0.31$ ,  $\mathbf{iii)} 0.75$  and  $\mathbf{iv)} 0.20$ .

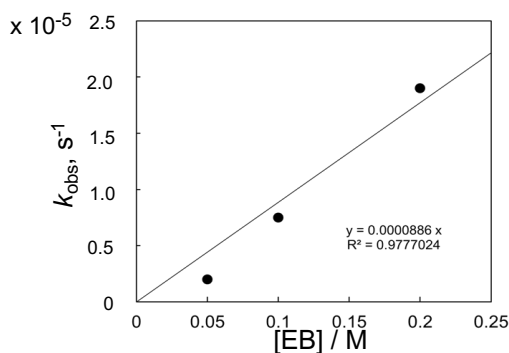


**Figure S50.** A plot of  $k_{\text{obs}}$ ,  $10^{-5} \text{ s}^{-1}$  against concentration of ethylbenzene [EB] / M in reactions of  $[\text{IV},\text{IV}]^{2+}$ .  $k' = k/2 = 4.4 \times 10^{-5}$ .

**Table S7.** Summary of the rate constant ( $k'$ ,  $\text{M}^{-1} \text{ s}^{-1}$ ).

substrate	$\text{BDE}_{\text{C-H}}$ kcal mol <sup>-1</sup> S6)	rate constant $k'$ , $\text{M}^{-1} \text{ s}^{-1}$	
		$[\text{IV},\text{IV}]^{2+}$	$[\text{IV},\text{IV}_1\text{H}]^{3+}$
	79	$2.3 \times 10^{-2}$	$1.2 \times 10^{-4}$
benzyl alcohol (BA)			
	81.6	$1.8 \times 10^{-3}$	$9.4 \times 10^{-5}$
cyclohexene (CH)			
	83.2	$2.0 \times 10^{-2}$	$1.1 \times 10^{-4}$
cumene (CU)			
	85.4	$8.8 \times 10^{-5}$	-
ethylbenzene (EB)			

## V. DFT Calculations

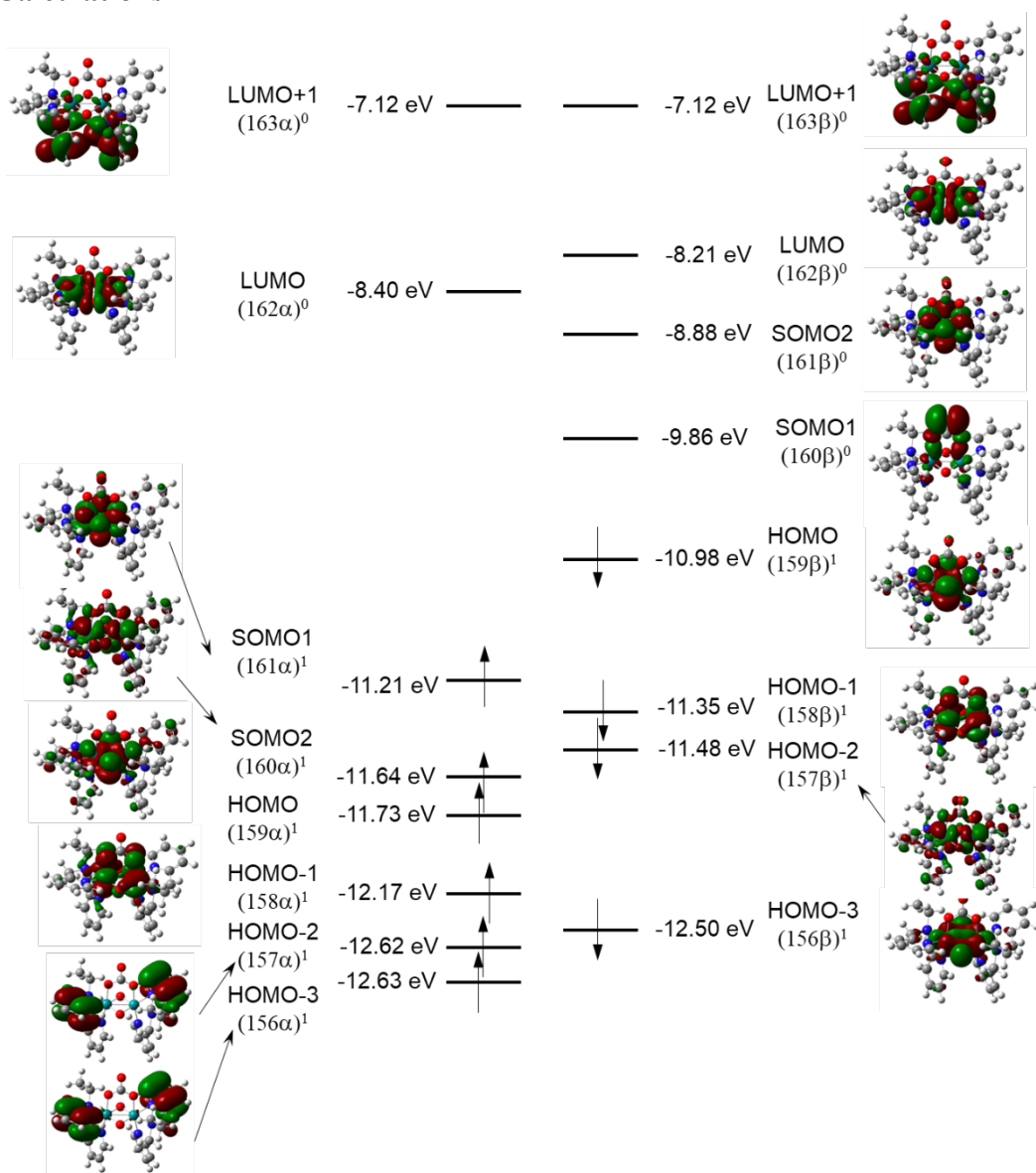


**Figure S51.** MO contributions of  $[IV,IV]^{2+}$  by DFT calculations shown at isovalue = 2 (charge 2, triplet).

**Table S8.** Comparisons of structural parameters of  $[\text{IV},\text{IV}]^{2+}$ .

	Theo.		Exp.	
Bond lengths / Å				
Ru-O1	1.993	1.987	1.905(3)	1.914(3)
Ru-O2	1.987	1.993	1.904(3)	1.919(3)
Ru---Ru	2.535		2.4261(3)	
Ru-O(carbonato)	2.147	2.147	2.031(3)	2.022(3)
Ru-N(amine)	2.188	2.186	2.147(3)	2.146(3)
Ru-N(py)2,5	2.099	2.099	2.091(3)	2.091(3)
Ru-N(py)3,6	2.064	2.064	2.076(3)	2.072(3)
O(coordinated)-C(carbonato)	1.288	1.288	1.311(5)	1.312(4)
C-O(carbonato)	1.358		1.228(5)	
Bond angles / °				
Ru1-O-Ru2	79.13	79.13	79.14(10)	78.53(10)
O1-Ru-O2	100.62	100.62	101.09(11)	100.93(11)
O1,2-Ru1,2-N(amine)1,4	169.70	169.70	167.12(13)	170.19(11)
O2,1-Ru1,2-N(amine)1,4	88.84	88.84	89.56(13)	91.59(13)
O1,2-Ru2,1-N(py)5,2	166.62	166.62	168.76(13)	167.47(13)
O1,2-Ru1,2-N(py)3,6	94.41	95.31	93.07(13)	95.53(12)
O1,2-Ru1,2-N(py)3,6	95.31	94.41	94.56(12)	92.23(13)
Ru-O(carbonato)-C	119.50	119.49	94.56(12)	92.23(13)
O(coordinated)-C-O(terminal)	116.47	116.47	122.0(2)	121.2(2)
O(coordinated)-C-O(coordinated)	127.06		120.8(3)	

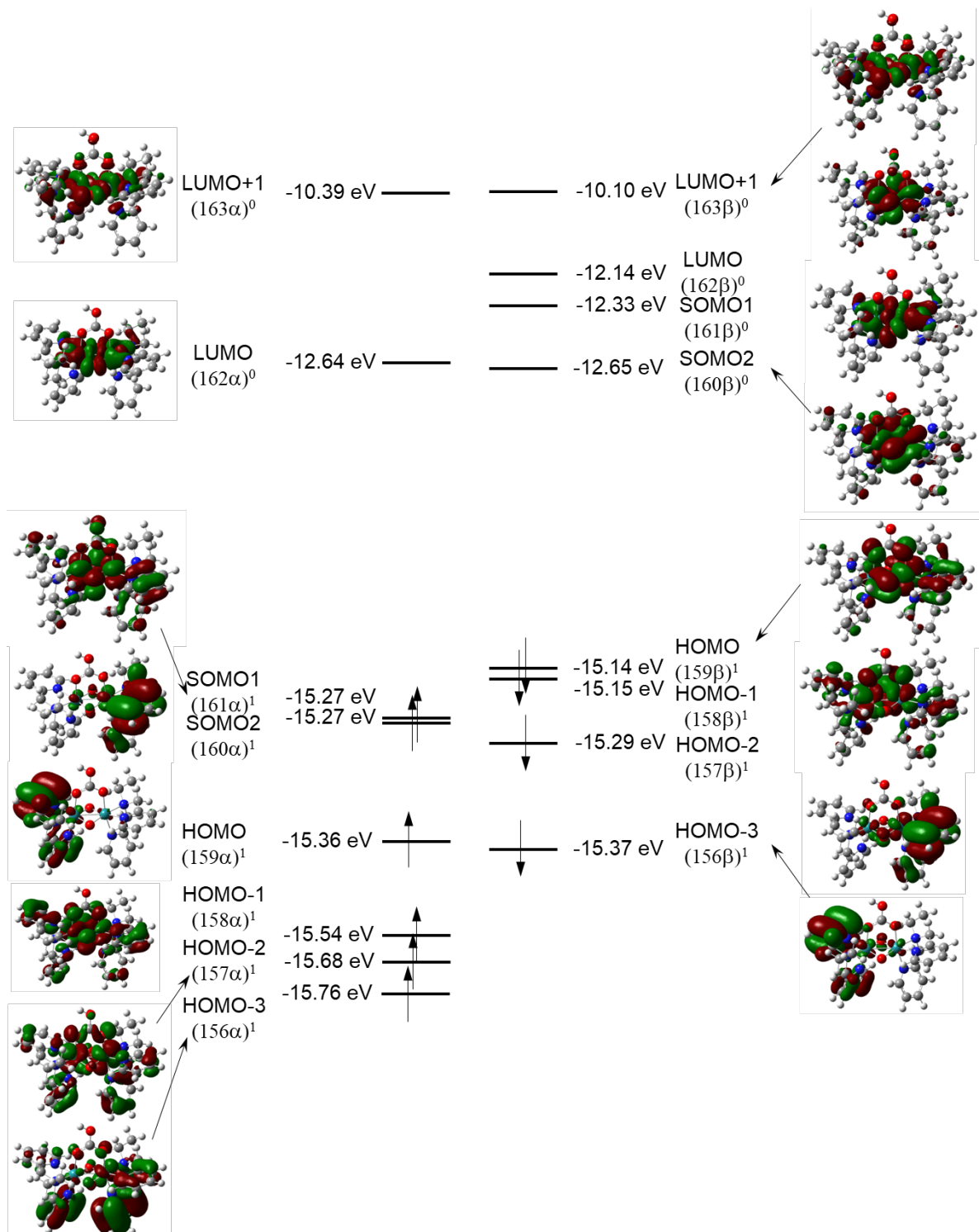


**Figure S52.** MO contributions of  $[IV,IV\_1H]^{3+}$  by DFT calculations shown at isovalue = 2 (charge 3, triplet).

**Table S9.** Comparisons of structural parameters of [IV,IV-1H]<sup>3+</sup>.

	Theo.		Exp.	
	Bond lengths / Å			
Ru-O1	2.077	1.907	1.918(2)	1.899(2)
Ru-O2	1.906	2.077	1.902(2)	1.914(2)
Ru---Ru		2.604		2.4389(3)
Ru-O(hydrogencarbonato)	2.114	2.095	2.069(2)	2.065(2)
Ru-N(amine)	2.152	2.148	2.130(3)	2.134(3)
Ru-N(py)2,5	2.109	2.111	2.078(3)	2.086(3)
Ru-N(py)3,6	2.075	2.074	2.047(3)	2.056(3)
O(coordinated)-C(bicarbonato)	1.304	1.291	1.265(4)	1.269(4)
C-OH(hydorgencarbonato)		1.343		1.297(4)
	Bond angles / °			
Ru1-O-Ru2	81.49	81.53	79.34(9)	79.53(8)
O1-Ru-O2	97.44	97.44	100.45(9)	100.47(9)
O1,2-Ru1,2-N(amine)1,4	170.23	170.25	167.97(11)	169.15(11)
O2,1-Ru1,2-N(amine)1,4	91.56	92.02	91.00(11)	90.51(11)
O1,2-Ru2,1-N(py)5,2	171.77	171.67	167.97(11)	168.23(11)
O1,2-Ru1,2-N(py)3,6	92.63	97.56	94.30(11)	95.07(11)
O1,2-Ru1,2-N(py)3,6	96.58	93.41	94.83(11)	94.29(11)
Ru-O(bicarbonato)-C	121.33	122.84	119.8(2)	120.2(2)
O(coordinated)-C-O(coordinated)		124.19		125.2(3)
O(coordinated)-C-OH(terminal)	119.72	116.09	119.0(3)	115.8(3)

## VI. References

- [S1] Y. Shimizu, S. Fukui, T. Oi, H. Nagao, *Bull. Chem. Soc. Jpn.* **2008**, *81*, 1285.
- [S2] T. Suzuki, K. Matsuya, T. Kawamoto, H. Nagao, *Eur. J. Inorg. Chem.* **2014**, 722.
- [S3] T. Suzuki, Y. Suzuki, T. Kawamoto, R. Miyamoto, S. Nanbu, H. Nagao, *Inorg. Chem.* **2016**, *55*, 6830.
- [S4] T. Misawa-Suzuki, S. Mafune, H. Nagao, *Inorg. Chem.* **2021**, *60*, 9996.
- [S5] O. V. Dolomanov, L. J. Bourhis, R. J. Gildea, J. A. K. Howard, H. Puschmann, OLEX2: A Complete Structure Solution, Refinement and Analysis Program, *J. Appl. Crystallogr.* **2009**, *42*, 339.
- [S6] Y.-R. Luo, Comprehensive Handbook of Chemical Bond Energies, *CRC, Boca Raton, FL*, 2007.